Magdalena Stelzer, BSc

Numerical Studies on the PLAXIS Jointed Rock Model

MASTER'S THESIS

to achieve the university degree of

Diplom-Ingenieurin

Master's degree programme: Civil Engineering, Geotechnics and Hydraulics

submitted to

Graz University of Technology

Supervisor

Ao.Univ.-Prof. Dipl.-Ing. Dr.techn. M.Sc. tit.Univ.-Prof.
Helmut Schweiger

Institute of Soil Mechanics and Foundation Engineering

Second supervisor
Dipl.-Ing. Patrick Pichler, BSc.

Graz, June 2015

AFFIDAVIT

I declare that I have authored this thesis independently, that I have not used other than the declared sources/resources, and that I have explicitly indicated all material which has been quoted either literally or by content from the sources used. The text document uploaded to TUGRAZonline is identical to the present master‘s thesis dissertation.

Date

Signature

Acknowledgement

There are many people who contributed to the success of my studies and finally this master thesis and I want to express my gratitude to all of them.

I want to thank Ao.Univ.-Prof. Dipl.-Ing. Dr.techn. M.Sc. tit.Univ.-Prof. Helmut Schweiger and Dipl.-Ing. Patrick Pichler, BSc who offered an excellent supervision and technical support of this thesis.

I would also like to thank my friends and colleagues, especially to those of the “Wasserbauzeichensaal der Technischen Universität Graz”. You made every single term of my studies to what they were – a diversified, interesting, of course informative but most of all an amazing and cheerful phase of my life, wherefrom I take countless great memories into those to come.

My warm thank goes to my family, who supported me from the day I decided to choose this field of study until the last word of this thesis. You kept me grounded in all situations and believed in me and my skills even if I didn’t.

Most of all I want to thank Christof, for being my motivating force and for helping me to enjoy life to the full, without losing the focus.

Kurzfassung

Das Jointed Rock Modell ist ein Materialmodell für zerklüfteten Fels als Kontinuum, welches zur Lösung von geotechnischen Problemen von der Finite Elemente Software „PLAXIS“ zur Verfügung gestellt wird. Diese Arbeit soll einen Überblick über das grundlegende Verhalten eines Jointed Rock Materials, sowie Empfehlungen zur Anwendung liefern. Durch die Analyse von Spannungszuständen und Versagensbildern eines Kragarmes werden elementare Erkenntnisse über das Materialverhalten gewonnen, welche auf die geotechnisch relevanten Strukturen eines Hanganschnittes und eines Tunnelvollausbruches angewendet werden. Fokus liegt dabei auf dem Einfluss des Fallwinkels der Trennflächen auf das resultierende Versagensbild. Das Versagen wird mittels φ/c-Reduktion und einer Lastaufbringung eingeleitet und die Ergebnisse untereinander verglichen. Die Ergebnisse der numerischen Berechnungen werden jenen von Simulationen mit einem zweiten Materialmodell für zerklüfteten Fels, sowie analytischen Berechnungen gegenübergestellt und verifiziert.

Abstract

The Jointed Rock model is a constitutive model for jointed rock as a continuum provided by the finite element software “PLAXIS” for the investigation of geotechnical problems. This thesis includes an overview of the general behaviour of Jointed Rock material as well as recommendations on the usage of the model. By analyzing the stress conditions and failure mechanisms of a cantilever structure elementary information on the material behaviour is obtained and applied on the geotechnical relevant structures of a cut slope and a full face tunnel excavation. Focus lies on the influence of the dip angle of the joints on the resulting failure mechanism. The failure of the structure is induced by a φ/c-reduction and a uniform vertical load. The calculation results are compared to each other and verified by the calculation output of a second material model for jointed rock and analytical calculations.

Table of contents

List of figures

List of tables

List of symbols and abbreviations

Capital letters

A	[m^2]	Area of the sliding plane/body
E	[N/m^2]	Young's modulus
G_2	[N/m^2]	Shear modulus perpendicular to plane 1 direction
G	[N]	Weight force of the rock body
K_0	[-]	Coefficient of earth pressure at rest

Small letters

c	[N/m^2]	cohesion
n	[-]	number of sliding planes
q_y	[N/m]	distributed load in y-direction
u	[m]	displacement of a FE node

Greek letters

α_1	[^{o}]	dip angle of sliding planes
α_2	[^{o}]	strike of sliding planes
β	[°]	slope inclination angle
β_{CS}	[°]	inclination angle of the cross section
γ	[N/m^3]	weight
φ	[^{o}]	friction angle
ψ	[°]	dilatancy angle
σ	[N/m^2]	normal stress
τ	[N/m^2]	shear stress
ν	[-]	Poisson's ratio

Abbreviations

FEM	Finite element method
JR	Jointed Rock
MC	Mohr Coulomb
UDSM	User defined soil model
Iso-JRMC	Jointed Rock model with overall Mohr-Coulomb failure criterion
FoS	Factor of safety

1 Introduction

In geotechnical engineering jointed rock masses often cause problems in planning and designing processes. It is not only difficult to gain sufficient knowledge about the joint properties concerning their geometry and mechanical parameters but the consideration of discrete jointing also requires high calculation efforts, leading to long processing times and high related costs. The Jointed Rock model is a continuous constitutive model provided by the finite element software PLAXIS that offers a simplified approach for problems including jointed rock material. Objective of the present thesis is to outline the basic behaviour of Jointed Rock material and to provide recommendations on the usage of this model.

Preliminary studies on a simple cantilever structure in equilibrium as well as in failure provide basic information on stress conditions, deformations and plasticity of a Jointed Rock mass. With the gained knowledge investigations on a cut slope and on a tunnel excavation problem are carried out, including detailed failure analyses and the influence of the dip angle, anisotropic behaviour, dilatancy and the initial stress state. To verify the numerical calculation output, comparative calculations with a user-defined soil model for PLAXIS as well as analytical calculations are performed.

Based on the findings from the computational analyses, recommendations for the usage of the PLAXIS Jointed Rock model are provided throughout the thesis.

2 Jointed rock as a continuum

In the designing processes of geotechnical problems jointed rock masses often lead to high calculation efforts, when intact rock and present joints are considered separately. The behaviour of the jointed rock mass is influenced by the strength properties and geometries of the discontinuities as well as by those of the intact rock material, hence a very sound understanding of the behaviour of the rock mass is required in order to choose an appropriate model for designing and analyzing purposes. If the joints have a small spacing and are parallel to each other, it is possible to simplify this problem by means of a continuum constitutive model for jointed rock. The finite element software PLAXIS offers the possibility to simulate jointed rock as a continuous mass. The jointed rock mass is modeled as a single material, combining the properties and characteristics of both, the intact rock and the discontinuities.

2.1 The PLAXIS Jointed Rock model

The PLAXIS Jointed Rock model (hereinafter referred to as “JR model”) is an anisotropic elastic, perfectly plastic material model that represents a continuum model for jointed rock. It combines the characteristics of its two main components, the intact rock and a maximum of three major joint directions (sliding planes). The intact rock acts as an elastic material and by assigning different elasticity properties transversal anisotropy (i.e. stratification) can be modelled. This behaviour is implemented by a transversely anisotropic elastic material stiffness matrix. The joint sets may have different strength properties with limited shear stress according to Coulomb’s criterion and a predefined limited tensile strength perpendicular to the sliding plane (Brinkgreve et al. 2014a).

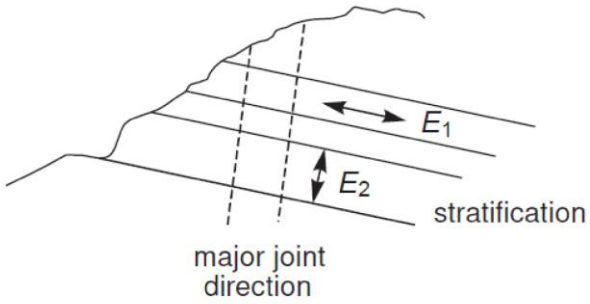

Fig. 1 PLAXIS Jointed Rock model (Brinkgreve et al. 2014a)

The application of the JR model is justified for material that shows parallel joint sets or joint families that are not filled with fault gauge. The spacing between the joints has to be small compared to the overall dimensions of the structure.

2.1.1 Material parameters

The PLAXIS Material Models Manual (2014) lists the following basic material parameters for the JR model:

- **Elastic parameters for intact rock**

E_1	[N/m^2]	Young's modulus for intact rock
ν_1	[-]	Poisson's ratio for rock as a continuum

- **Anisotropic elastic parameters „Plane 1 direction" (e.g. stratification direction)**

E_2	[N/m^2]	Young's modulus perpendicular to "Plane 1
ν_2	[-]	Poisson's ratio perpendicular to "Plane 1" direction
G_2	[N/m^2]	Shear modulus perpendicular to "Plane 1" direction

- **Shear failure according to Coulomb in a maximum of three directions with parameters**

c_i	[N/m^2]	cohesion
φ_i	[°]	friction angle
ψ_i	[°]	dilatancy angle
$\sigma_{t,i}$	[N/m^2]	tensile strength

- **Definition of joint directions**

n	[-]	number of joint directions
$\alpha_{1,i}$	[°]	dip angle ($-180 \leq \alpha_{1,i} \leq 180$)
$\alpha_{2,i}$	[°]	strike ($\alpha_{2,i}$ = 90 in PLAXIS 2D)

The Young's modulus E_1 and the Poisson's ratio ν_1 are the elastic parameters of the intact rock as a continuum according to Hooke's law. Optional anisotropy due to stratification is represented by the parameters E_2 and ν_2, which define the stiffness of the mass perpendicular to the stratification direction. The shear stiffness in the direction of anisotropy is explicitly defined by the user by means of the shear modulus G_2.

For each sliding plane i the strength parameters c_i, φ_i and ψ_i are defined. Maximum shear strength is defined according to Coulomb's criterion. Tensile stresses perpendicular to the sliding planes are limited according to the tension cut-off criterion that is determined by the user defined tensile strength σ_t.

For a plane *i* with local (n,s,t)-coordinates, the yield functions are defined as:

$$f_i^c = |\tau_s| + \sigma_n \tan_{\varphi,i} - c \qquad \text{(Coulomb)} \tag{1}$$

$$f_i^t = \sigma_n - \sigma_{t,i} (\sigma_{t,i} \leq c_i \, cot \, \varphi_i) \qquad \text{(Tension cut-off)} \tag{2}$$

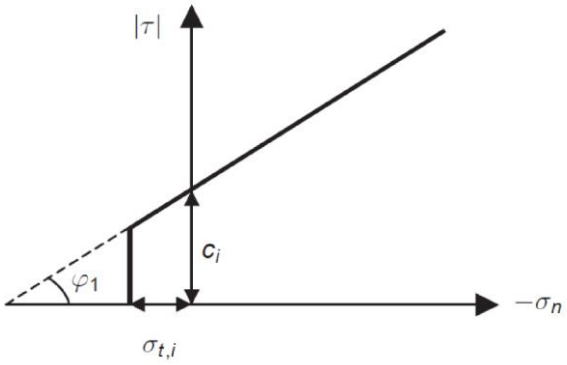

Fig. 2 Full yield criterion for an individual plane *i* (Brinkgreve et al. 2014a)

The joint directions are defined by the means of the two parameters α_1 for the dip angle and α_2 for the strike. A minimum of one and a maximum of three major joint directions are to be defined by the user. In the present thesis simulations are run in 2D only. In this case no strike (α_2) has to be defined as it is set to 90° by default. Furthermore it holds:

$$(-\alpha_1) \equiv 180 - \alpha_1 \tag{3}$$

The definition of the angles α_1 and α_2 is shown in Fig. 3.

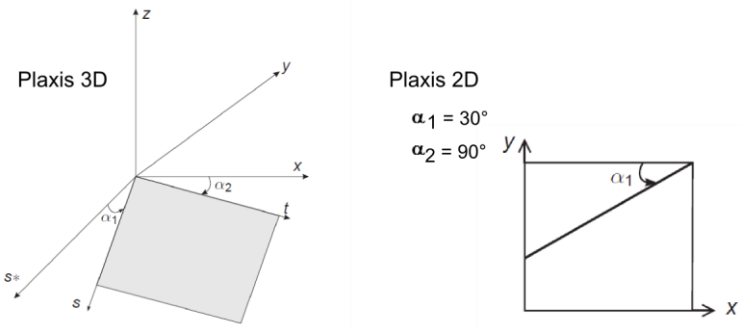

Fig. 3 Definition of dip angle and dip direction (Brinkgreve et al. 2014a)

In case of anisotropic behaviour, the first plane also corresponds to the plane of anisotropy (“plane-1”-direction).

Further information about the JR model is provided by the PLAXIS Material Models Manual 2014 (Brinkgreve et al. 2014a).

3 Preliminary investigations on a cantilever

To investigate the general behaviour of a material with the JR model assigned, the simple structure of a cantilever is modelled. A selection of representative plots of the calculation output shows stress distributions, deformations and plastic sliding for varying dip angles α_1. The calculation output is presented separately for the structure in equilibrium and the structure after failure.

3.1 Geometry and mesh coarseness

The finite element model of the cantilever is a plane strain model with 1526 15-noded elements. The rock body is 15 m in width and 5 m in height (b:h = 3:1). It is clamped at x = 15 m and free at all other boundaries.

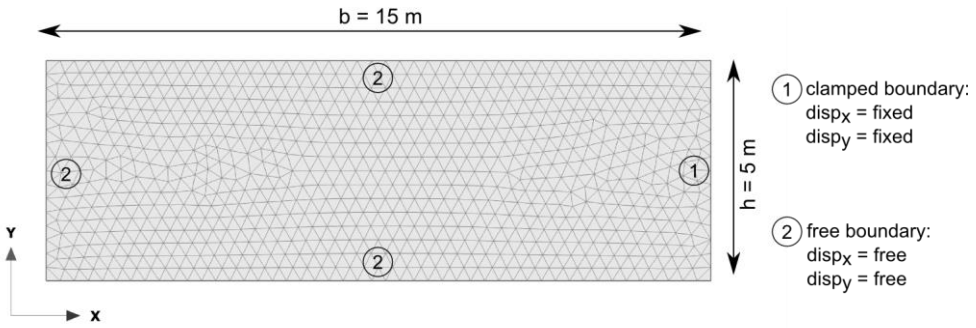

Fig. 4 Geometries and mesh coarseness of the FEM model of a cantilever

3.2 Material properties

The intact rock mass of the body is defined to be isotropic-elastic material. It holds:

$$E_1 = E_2 \tag{4}$$

$$\nu_1 = \nu_2 \tag{5}$$

In this case the shear modulus perpendicular to the “plane 1”-direction G_2 is related to the Young’s modulus by means of Poisson’s ratio:

$$G_2 = \frac{E_1}{2(1+\nu_1)} \tag{6}$$

To guarantee equilibrium in the initial state of the structure, the cohesion of 1500 kN/m² was determined through an iterative procedure. Due to gravity loading the rock body deflects in negative y-direction. This deflection causes tensile stresses on the upper horizontal boundary of the structure. To ensure that the structure can sustain these

initial tensile stresses, the sliding plane is assigned a tensile strength that corresponds to the cohesion.

$$\sigma_t = c = 1500\ kN/m^2 \tag{7}$$

The structure has one major joint direction, i.e. n = 1. To investigate the influence of the dip angle it is varied as follows:

$$\alpha_1 = 0°/\ 30°/\ 45°/\ 60°/\ 90°/\ 120°/\ 135°/\ 150°$$

All material properties are shown in Tab. 1.

Tab. 1 Material properties of the cantilever

Parameter	Unit	Intact rock	Sliding plane
γ	[kN/m³]	24	-
E_1	[kN/m²]	$3.0*10^5$	-
E_2	[kN/m²]	$3.0*10^5$	-
ν_1	[-]	0.2	-
ν_2	[-]	0.2	-
G_2	[kN/m²]	$1.25*10^5$	-
c_{ref}	[kN/m²]	-	1500
φ	[°]	-	25
ψ	[°]	-	0
α_1	[°]	-	varies
σ_t	[kN/m²]	-	1500

3.3 Behaviour of a JR body in equilibrium

To show the behaviour of a JR body in equilibrium, the FEM simulation is run with one calculation phase only. By defining the calculation type as “gravity loading” the self-weight of the body is activated and no additional load is acting on the structure. In this chapter a selection of representative simulation results for stress distributions and deformations are presented.

Tab. 2 Calculation phases of the cantilever simulation

Phase nr.	Phase ID	Calculation type	Loading type
Phase 0	Initial phase	Gravity loading	Staged construction

Note: *Arc length control* is switched *off* (see section 4.5 Arc length control).

3.3.1 Tension cut-off

Referring to chapter 2.1.1, tensile stresses perpendicular to the sliding plane are limited by a predefined tensile strength with the tension cut-off criterion. The distribution of normal stresses along a cross section that has the same inclination angle as the sliding plane (i.e. $\beta_{cs} = \alpha_1$) verifies that this criterion is fulfilled. Fig. 5 shows the distribution of normal stresses σ_n along a cross section for $\alpha_1 = 90°$. The maximum tensile normal stress is 1500 kN/m^2 and therefore it holds:

$$\sigma_{n,max} \leq \sigma_t \tag{8}$$

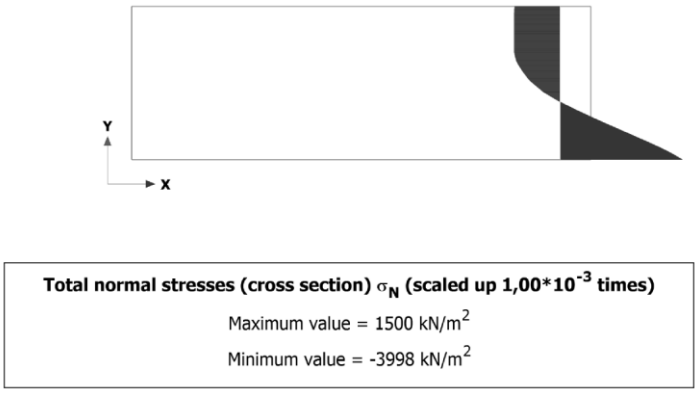

Fig. 5 Normal stresses perpendicular to the sliding plane: $\alpha_1 = 90°$, $\sigma_{t,n,max}$ =1500 kN/m^2

3.3.2 Cartesian stresses

Fig. 6 shows the stress distribution of the cartesian normal stresses σ_{xx}, σ_{yy} as well as the cartesian shear stresses τ_{xy} for a JR body with a dip angle of $\alpha_1 = 60°$. Considering the stresses in x-direction it is visible that tensile stresses develop for y > 2.5 m, whereas compressive stresses develop for y < 2.5 m. In all three plots the stress distributions close to the upper right corner of the structure indicate a dependency on α_1 as they show an orientation along the sliding plane. Due to the gravitational loading and the resulting deflection of the structure, tensile stresses develop perpendicular to the joints and flexural cracking occurs.

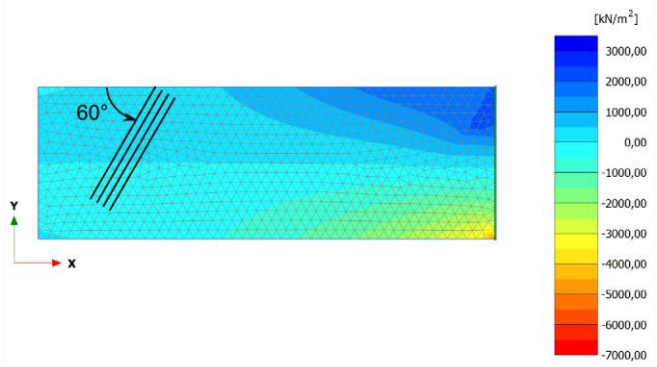

Cartesian normal stresses σ_{xx}
Maximum value = 3269 kN/m²
Minimum value = -6659 kN/m²

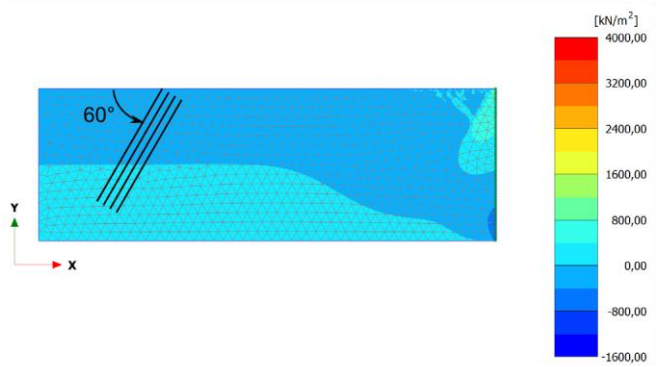

Cartesian normal stresses σ_{yy}
Maximum value = 3965 kN/m²
Minimum value = -1420 kN/m²

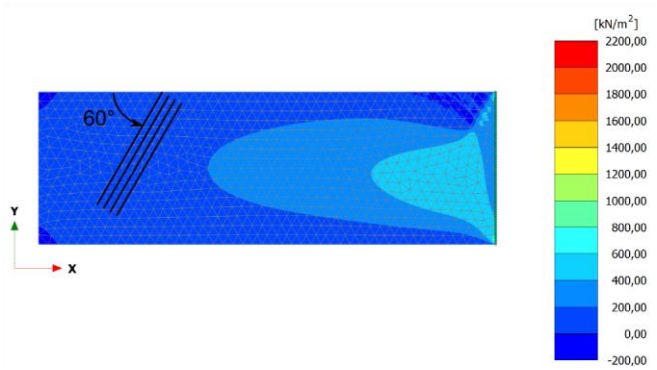

Cartesian shear stresses τ_{xy}
Maximum value = 2147 kN/m²
Minimum value = -189.3kN/m²

Fig. 6 Distribution of cartesian normal stresses σ_{xx}, σ_{yy} and cartesian shear stresses τ_{xy} for α_1 = 60°

The influence of α_1 is furthermore shown in the following two graphs. The development of normal stresses in x- and y-direction depending on the total load level (ΣM_{Stage}) in a stress point close to the upper boundary of the clamping with the coordinates (14.80/4.25) is plotted for varying α_1.

Tensile stress in x-direction increases for all α_1 with increasing load level. Non-strictly monotonously rising sections of the curve indicate that plastic sliding occurs and/or the tension cut-off criterion that limits maximum tensile stresses perpendicular to the sliding plane is valid. The latter is very well represented for α_1 = 90°. In this case the cartesian

stresses in x-direction correspond to the tensile stresses perpendicular to the sliding plane, therefore they do not exceed a value of 1500 kN/m^2 (Fig. 7).

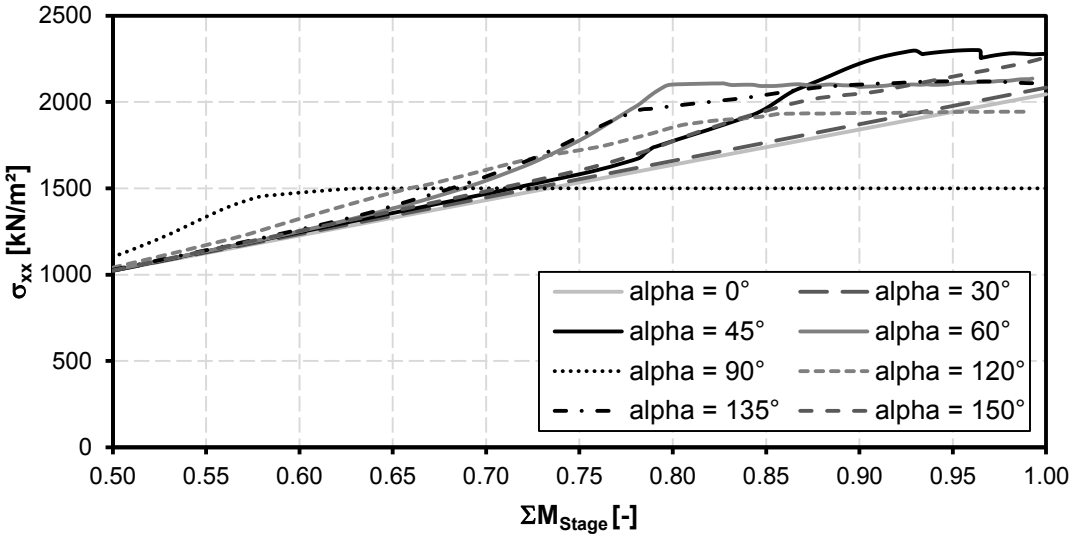

Fig. 7 Cartesian normal stresses in x-direction σ_{xx} for varying α_1 in a stress point (14,80/4,25)

Tensile stresses in y-direction increase for α_1 = 60°, 45°, 135°, 30° and 0°, whereas they decrease with increasing load level for α_1 = 120°, 90° and 150°. For the latter they result in compressive stresses (Fig. 8).

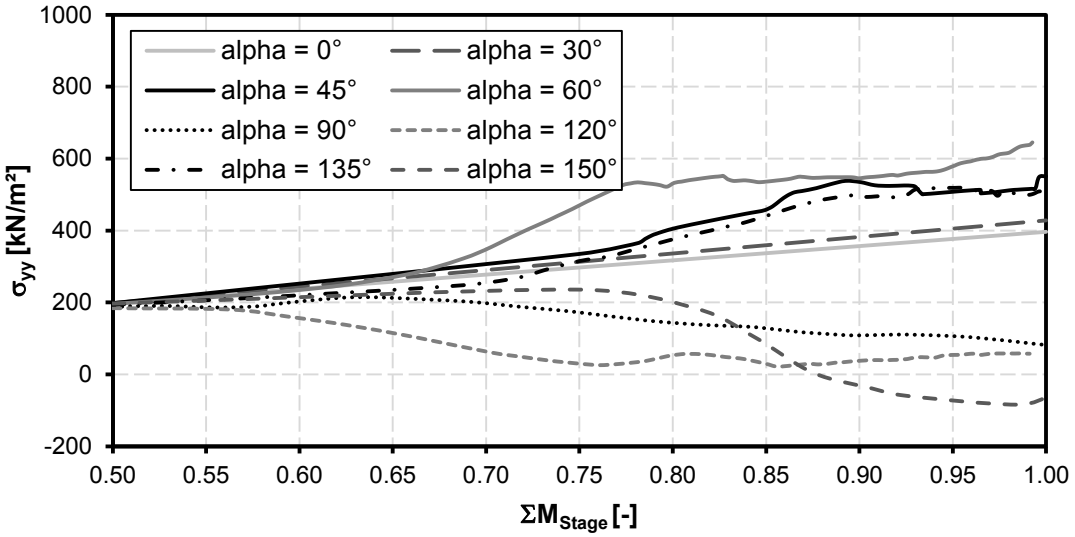

Fig. 8 Cartesian normal stresses in y-direction σ_{yy} for varying α_1 in a stress point (14,80/4,25)

3.3.3 Deformation

According to the given boundary conditions, maximum deformation $|u_{max}|$ occurs at the dip of the cantilever (x = 0 m) and no failure mechanism develops since the structure is in equilibrium.

Fig. 9 presents the maximum deformation for varying α_1. The smallest deformation results for horizontal jointing. The values increase slightly for steeper inclinations of the joints and the maximum value is obtained for vertical jointing.

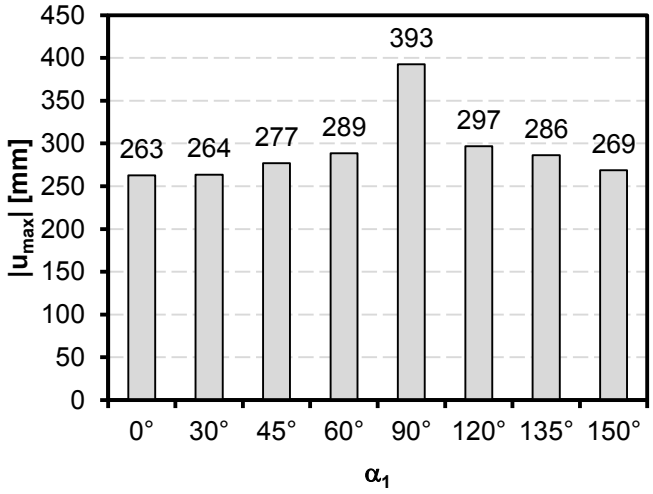

Fig. 9 Maximum deformation $|u_{max}|$ for varying α_1

3.3.4 Failure points and tension cut-off points

Plastic sliding occurs as soon as the maximum shear strength, according to Coulomb, is reached. In the PLAXIS Output this state is indicated by so called failure points. The program also marks all stress points that have reached limited tensile strength perpendicular to the sliding plane as tension cut-off points. The rock body in Fig. 10 shows both types of plastic points for a dip angle of α_1 = 60°. Due to flexural bending high tensile stresses develop transversely to the sliding planes and flexural cracks develop, as indicated by plastic points. Additionally, the formation of a sliding surface parallel to the jointing can be observed.

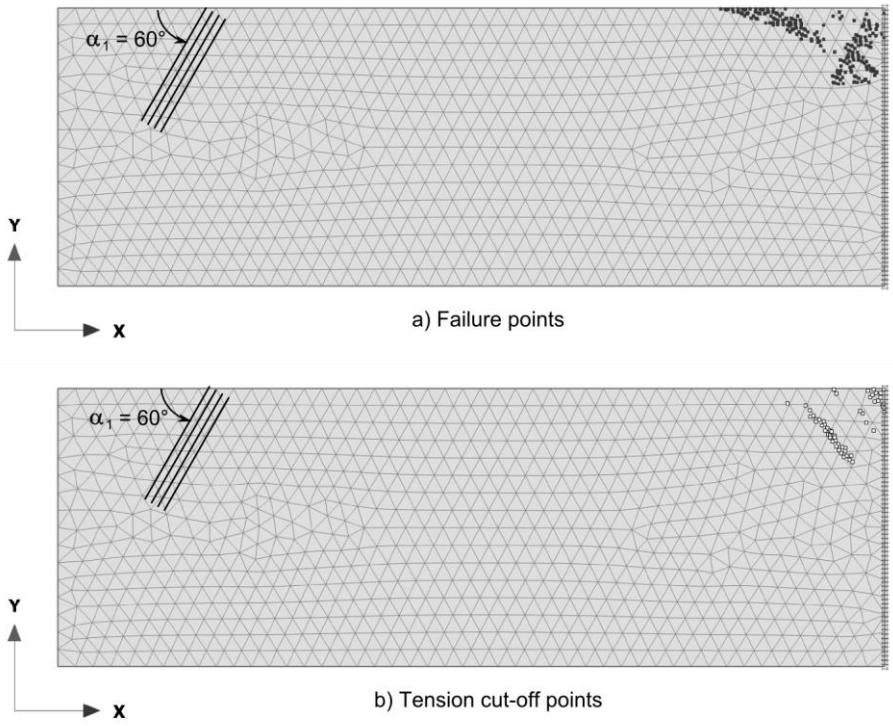

Fig. 10 Failure points and tension cut-off points for α_1 = 60°, ΣM_{Stage} = 1.00

3.4 Behaviour of a Jointed Rock body in failure

To evoke the collapse of the structure, a uniform vertical load q_y acts in negative y-direction on the upper horizontal boundary (y = 5 m). The required magnitude of q_y to reach failure differs for varying α_1. In the following sections the failure mechanism is discussed by interpreting the deformed mesh and the plastic points of the structure. The results are presented for α_1= 60° and 150°.

3.4.1 Deformation

The deformations after failure provide results for qualitative considerations only. A large scale of the deformed mesh enhances the effect of a good visualization to which failure mechanism the structure will deform. For α_1 = 60° a triangular body starting from the upper boundary of the clamping forms as it is indicated by a dashed triangle in Fig. 11. Compressive stresses in the lower part close to the fixed boundary are represented by a folding pattern. The shortest side *a* of the triangle is parallel to the jointing. The total load level at the end of the calculation results to ΣM_{Stage} = 0.61.

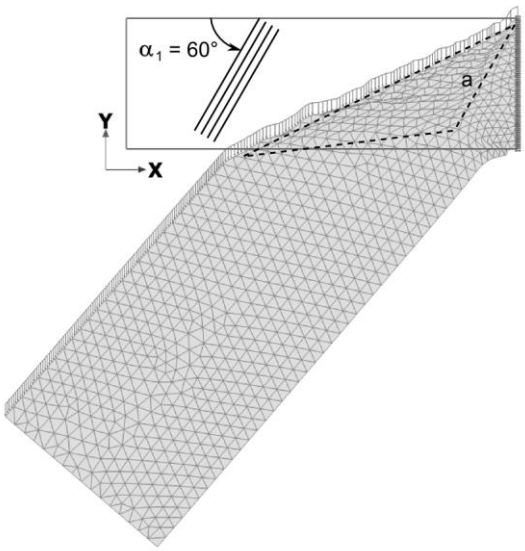

Fig. 11 Deformed mesh for $\alpha_1 = 60°$, $q_y = -200.00$ kN/m/m, $\Sigma M_{Stage} = 0.61$

3.4.2 Failure points and tension cut-off points points

Plasticity develops transversely to the dip angle of the joints. The four plots below show the formation of cracks transversal to the joint direction. Failure points (Fig. 12 a and Fig. 13 a) occur along with tension cut-off points (Fig. 12 b and Fig. 13 b). The endings of the individual cracks form a surface of the failure body that is parallel to the dip angle α_1. For other dip angles the behaviour pattern is similar, indicating that this behaviour is characteristic for a JR material that is in a failure state (see Appendix).

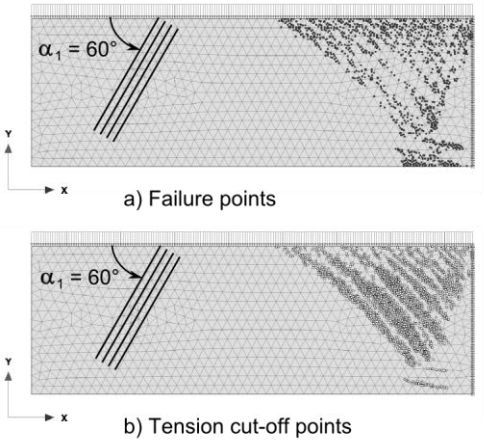

Fig. 12 Plastic points, $\alpha_1 = 60°$, $q_y = -200.00$ kN/m/m, $M_{Stage} = 0.61$

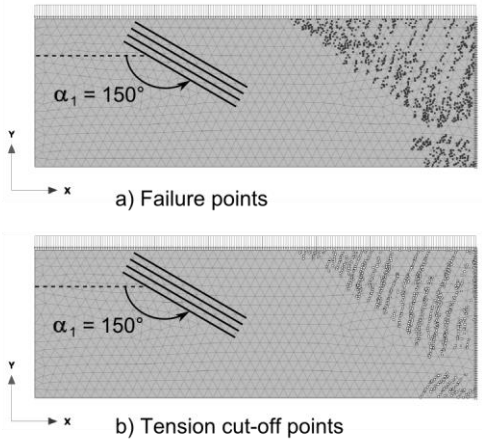

Fig. 13 Plastic points, $\alpha_1 = 150°$, $q_y = -200.00$ kN/m/m, $M_{Stage} = 0.46$

3.5 Conclusions

The behaviour of a JR cantilever structure in equilibrium is investigated to visualize the stress conditions in a simple JR structure. Gravitational loading leads to a deflection of the structure in negative y-direction, resulting in high tensile stresses in the upper part and compressive stresses in the lower part of the structure. Stress concentrations occur in transversal direction to the jointing, thus the shear strength as well as tensile strength of the sliding planes significantly influence the stability of the structure. By investigating maximum deformations and the location of plastic points, the significance of the influence of α_1 is pointed out.

The mentioned conditions and the further development of a JR structure is better visible when considering a structure after failure due to a uniform vertical load acting on the upper horizontal boundary. Flexural cracks transversal to the jointing develop and a sliding body is formed, showing one sliding surface parallel to the jointing.

The cantilever structure is a purely academic example to gain knowledge about the basic behaviour of the JR material model. Based on these findings, structures that are of more practical relevance are to be analyzed.

4 Investigations on a cut slope

To investigate the behaviour of a JR material on a simple structure that is relevant in soil and rock mechanical engineering, numerous simulations on a cut slope are performed and analyzed. Whereas the stress development in a JR mass was discussed in the previous chapter, the present chapter investigates the failure mechanism depending on the dip angle α_1 in more detail. In a first set of analyses the collapse of the structure is induced by executing a φ/c-reduction and the failure mechanism due to a uniform load on the edge of the slope is investigated in a second set. Focus lies on the influence of the dip angle of the sliding plane α_1. The effect of the use of the "arc length control" application in the calculation process will also be discussed. In the last section of this chapter a comparison with an additional Mohr Coulomb failure criterion for the intact rock, which is a user defined soil model (UDSM) for jointed rock, is presented.

4.1 Geometry and mesh coarseness

The finite element geometry model is 100 m in width and 50 m in height. The cut slope is constructed in a single excavation step and has a depth of 25 m with an inclination of β = 50° to the x-axis. The bottom horizontal boundary is fixed in x- and y-direction, whereas displacements in y-direction are possible at the two vertical boundaries (Fig. 14). The FEM model is a plane strain model consisting of 2810 15-noded elements. The mesh has a refined coarseness in the area around the slope's surface (Fig. 15).

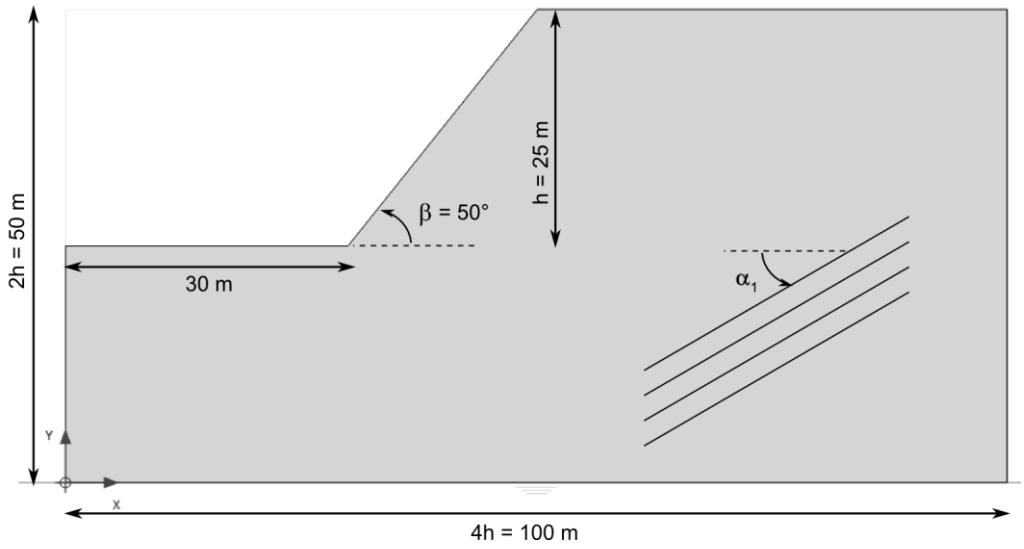

Fig. 14 Geometries of the FEM model of the cut slope

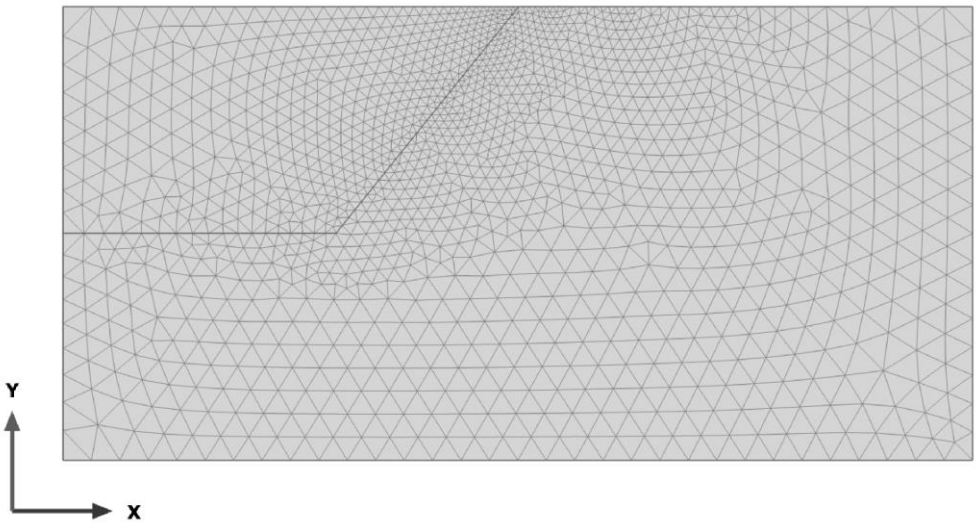

Fig. 15 FEM mesh of the cut slope: 2810 15-noded elements

4.2 Material properties

For this study one material set with varying dip angles is investigated. There is one set of sliding planes only, i.e. n = 1, and the dip angle α_1 is varied as follows:

$$\alpha_1 = 0° / 30° / 45° / 60° / 90° / 120° / 135° / 150°$$

The strength properties of the sliding planes and elasticity properties of the intact rock are the same for all material sets, which leads to comparable results. To ensure equilibrium after the initial and excavation phase in all cases, the cohesion of the sliding plane is set to the high value of c = 100 kN/m².[1] The intact rock is defined to be elastic isotropic (see also chapter 3.2). Tab. 3 shows a list of all user defined material parameters, other parameters are default parameters.

[1] The purpose of this simulation is to visualize the basic behaviour of the PLAXIS Jointed Rock material model rather than simulating a case study. For the latter the choice of the joints' strength parameters is to be based on a sound mechanical understanding of the present discontinuities. See also *Rock Slope Engineering*, Hoek & Bray (1981).

Tab. 3 Material properties of the cut slope

Identification	Unit	Value
Identification	[-]	JR
Material model	[-]	Jointed rock
Drainage type	[-]	Non-porous
γ	[kN/m³]	20.00
E_1	[kN/m²]	20000.00
ν_1	[-]	0.30
E_2	[kN/m²]	20000.00
ν_2	[-]	0.30
G_2	[kN/m²]	7692.00
Number of planes	[-]	1 plane
c_{ref}	[kN/m²]	100.00
φ	[°]	20.00
ψ	[°]	0.00
α_1(alpha 1)	[°]	varies
Tension cut-off	[-]	Yes
σ_t	[kN/m²]	0.00
K_0 determination	[-]	Manual
$K_{0,x}$	[-]	1.00

4.3 Failure mechanisms

The failure mechanism of the structure is investigated using two different approaches. By introducing a calculation phase of the type *Safety,* the failure mechanism, due to a φ/c-reduction, is analyzed. In another set of simulations the collapse of the structure is induced by a uniform load that is applied on the upper horizontal boundary of the structure.

The numerical simulation consists of three calculation phases as listed in Tab. 4. Phase 0 (Initial phase) and phase 1 (excavation) are the same for both sets of simulations. Phase 2 is a safety calculation in the first and a plastic calculation with a uniform vertical load acting on the slope in a second set of simulations.

Tab. 4 Calculation phases for failure analyses of a JR slope

Phase nr.	Phase ID	Type
Phase 0	Initial phase	K_0-procedure
Phase 1	Excavation	Plastic
Phase 2	Safety / load	φ/c-reduction / plastic

In general failure mechanisms of jointed rock slopes can be categorized in the following types (Goodman 1998, Graz University of Technology, Institute for Rock Mechanics and Tunneling 2007):

- Parallel sliding of a rock body (Fig. 16 a)
- Sliding of a rock wedge (Fig. 16 b)
- Toppling (Fig. 16 c)
    - Flexural toppling
    - Block toppling
    - Block-flexure toppling
- Planar buckling of rock layers or rock pillars (Fig. 16 d)
- Rock slumping (Fig. 16 e)
    - Flexural slumping
    - Block slumping

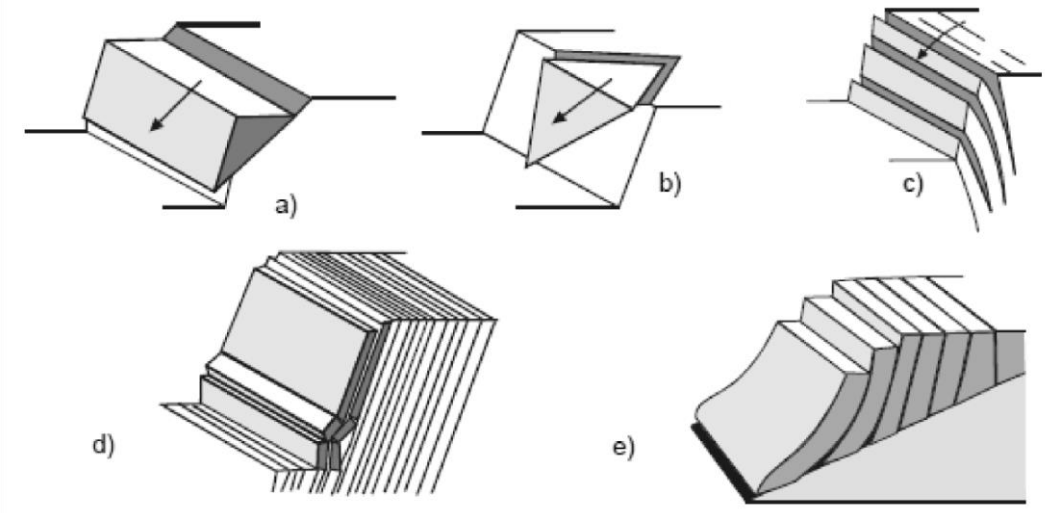

Fig. 16 Failure mechanisms of jointed rock slopes (Graz University of Technology, Institute for Rock Mechanics and Tunneling 2007)

The type of failure representing the governing mechanism depends on the mechanical properties such as cohesion and friction angle of the joints, as well as on the kinematical properties, such as the number of joint families with dip angles and the slope inclination. For the types *sliding of a rock wedge* and *rock slumping* a minimum of two sliding planes is required ($n \geq 2$). In the present FEM model only one set of parallel

joints is present (n = 1). Hence, the decisive mechanisms are *parallel sliding of a rock body*, *flexural toppling* and *planar buckling,* depending on α_1.

4.3.1 Parallel sliding

4.3.1.1 *Analytical solution for the factor of safety*

For verification purposes the FoS for the cut slope with $\alpha_1 = 30°$ is determined analytically. Equation (9) and Fig. 17 present the analytical approach to determine the limit equilibrium for parallel sliding along a joint with a cohesion *c* and a friction angle φ:

$$\eta = \frac{c * A_{SP}}{G * sin\alpha} + \frac{tan\varphi}{tan\alpha} \tag{9}$$

With A_{SP} [m^2] … surface area of the sliding plane

G [N] … dead weight of the sliding mass under gravitational loading

α [°] … dip angle of the joint

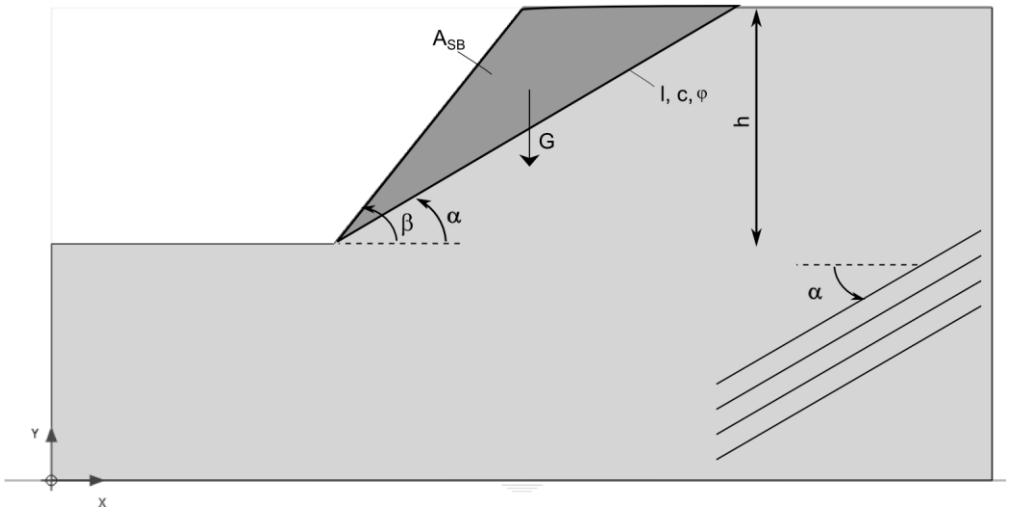

Fig. 17 Parameters for the analytical solution of the FoS of a sliding body

The parameters for the analytical determination of the slope stability are listed in Tab. 5.

Tab. 5 Parameters for the analytical determination of the slope stability

Idendification	Value	Unit	Description
α	30	[°]	Dip angle sliding plane
β	50	[°]	Slope inclination
h	25	[m]	Depth of the cut slope
A_{SB}	279	[m²]	Area of the sliding body
γ	20	[kN/m³]	Soil weight
l	50	[m]	Length of the sliding plane
c	100	[kN/m²]	Cohesion of the sliding plane
φ	20°	[°]	Friction angle of the sliding plane

The dead weight of the sliding body is calculated to:

$$G = \gamma * A_{SB} \tag{10}$$

$$= 20 * 279$$

$$= 5580.00\ kN$$

The factor of safety for this structure therefore results in:

$$\eta = \frac{c * A_{SP}}{G * sin\alpha} + \frac{tan\varphi}{tan\alpha} \tag{11}$$

$$= \frac{100 * 50 * 1}{5580 * sin30} + \frac{tan20}{tan30}$$

$$= 2.42$$

4.3.1.2 *Failure due to a φ/c – reduction*

The numerical determination of the factor of safety is done by performing a φ/c-reduction. Therefore, a staged construction consisting of three calculation phases is simulated. The initial state is computed by the K_0-procedure and the construction of the cut slope follows in a plastic calculation in phase 1. To determine the factor of safety (FoS) and the failure type a φ/c-reduction is performed in the last calculation phase:

$$FoS = \frac{c_{available}}{c_{failure}} = \frac{tan\varphi_{available}}{tan\varphi_{failure}} \tag{12}$$

Tab. 6 Calculation phases for safety analysis of a JR slope

Phase nr.	Phase ID	Calculation type	Loading type
Phase 0	Initial phase	K_0-procedure	Staged construction
Phase 1	Excavation	Plastic	Staged construction
Phase 2	Safety	φ/c-reduction	Incremental multipliers

Note: Arc length control is switched *off* in phase 0 and phase 1 (see section 4.5 Arc length control).

Fig. 18 shows plots of the plastic points (failure and tension cut-off points) and the deformed mesh of the structure at the end of phase 2 for a dip angle of $\alpha_1 = 30°$. Both plots indicate that a triangular body moves parallel to the sliding plane in negative y-direction. A sliding plane from the ground level to the toe of the slope is formed parallel to the defined joint inclination of 30°. The downwards movement of the body leads to high tensile stresses and therefore a concentration of tension cut-off points. The deformed mesh is shown in Fig. 18 c. The factor of safety computes to FoS = 2.53.

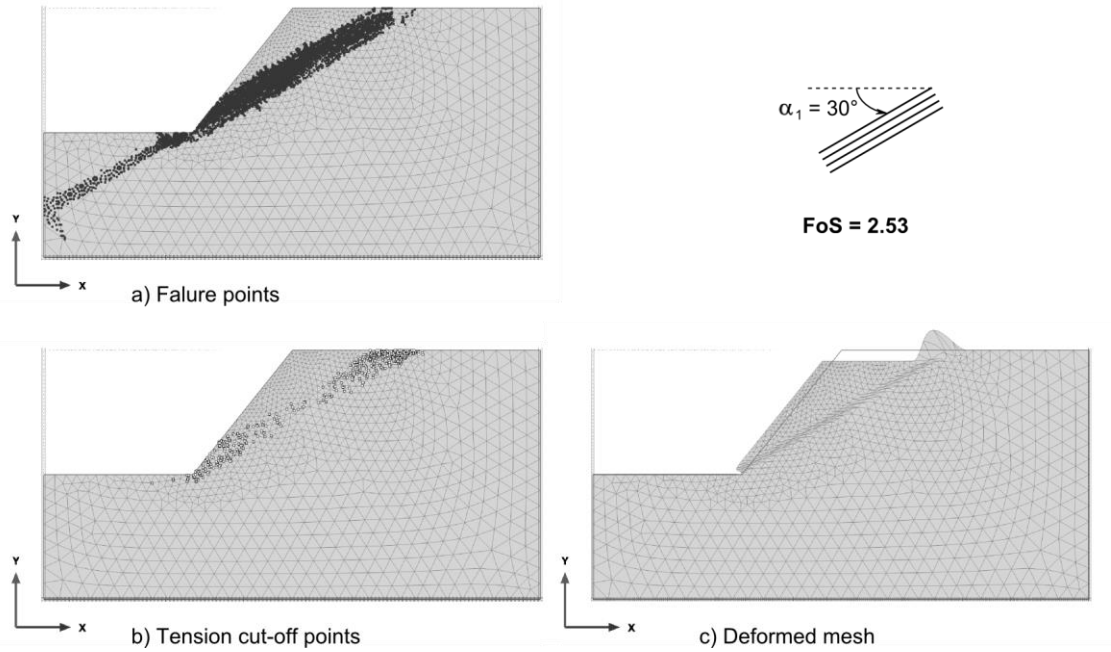

Fig. 18 φ/c-reduction: plastic points and deformed mesh for $\alpha_1 = 30°$, FoS = 2.53

The difference between the analytical and the numerical results for the FoS is 0.11 (equation (13)), which corresponds to a numerical result that is 4.5 % higher than the analytical one.

$$\Delta = |FoS - \eta| \tag{13}$$

$$= |2.53 - 2.42| = 0.11$$

The numerical calculation output is strongly dependent on the mesh coarseness. A simulation with a refined FEM mesh (18,734 elements) delivers a FoS of 2.40, which corresponds to a difference of 0.02 (equation (14)), indicating a good accordance with the analytical result. Failure points, tension cut-off points, and the deformed mesh of the structure are shown in Fig. 19.

$$\Delta_{ref} = |FoS - \eta| \tag{14}$$

$$= |2.40 - 2.42| = 0.02$$

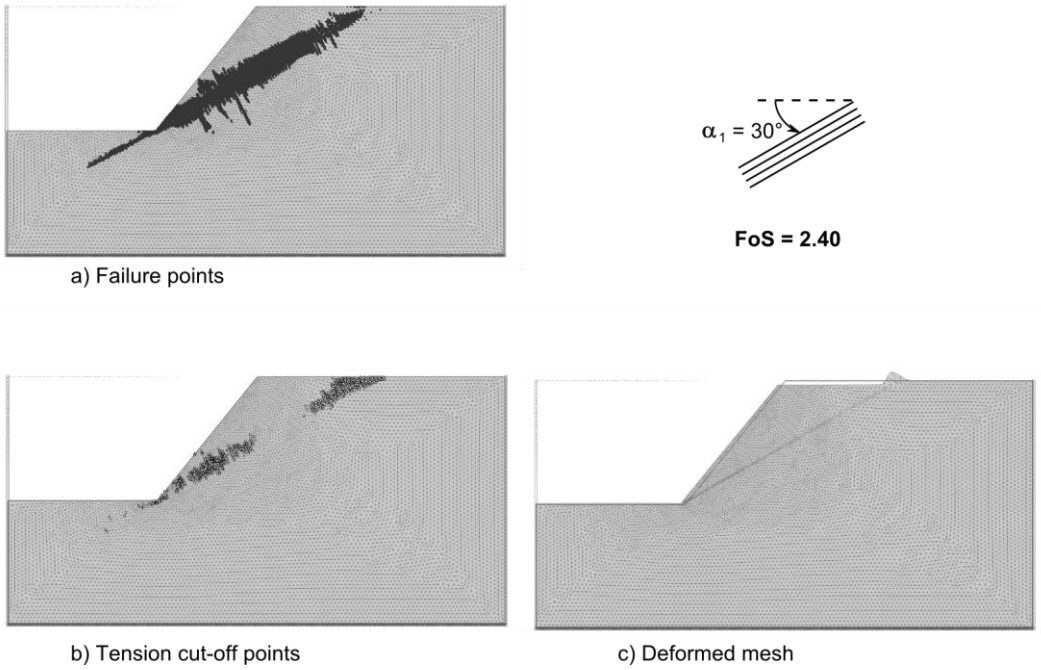

Fig. 19 φ/c-reduction with 18,734 elements: plastic points and deformed mesh for α_1 = 30°, FoS = 2.40

4.3.1.3 *Failure due to a uniform load*

A uniform vertical load q_y = 1000 kN/m^2 with a length of 20 m is applied on the edge of the cut slope to trigger failure after the excavation phase (Fig. 20 and Tab. 7).

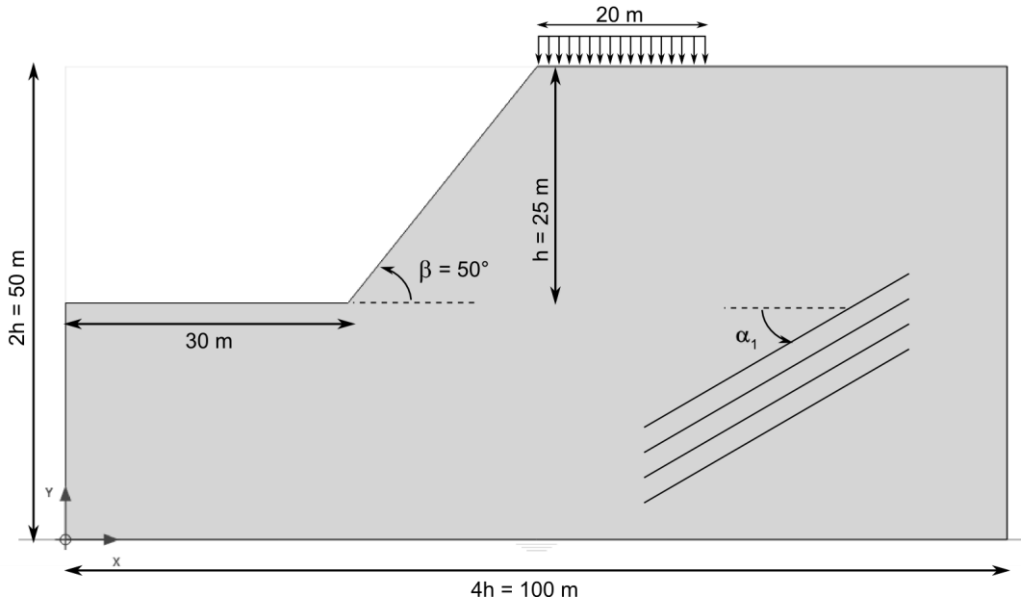

Fig. 20 System geometries and uniform load q_y

Tab. 7 Calculation phases for failure due to a uniform vertical load

Phase nr.	**Phase ID**	**Calculation type**	**Loading type**
Phase 0	Initial phase	K0-procedure	Staged construction
Phase 1	Excavation	Plastic	Staged construction
Phase 2	Load	Plastic	Staged construction

Note: Arc length control is switched *off* in all calculation phases (see section 4.5 Arc length control).

Fig. 21 shows the plastic points as well as the deformed mesh of the structure at the end of phase 2 for α_1 =30°. The distribution of plastic points results in a triangular body with its longest side parallel to the joint direction. The characteristic behaviour of JR structures discussed in chapter 3.4.2 is furthermore visible in this structure. Due to the applied load, plastic sliding occurs in transverse direction to the jointing. As the failure body moves towards the excavation, tensile stresses develop in the upper part at the end of q_y, visualized by a concentration of tension cut-off points (Fig. 21 b). The deformed mesh is shown in Fig. 21 c. As already discussed in chapter 3.4.2, cracks develop due to deflection, visualized by plastic points.

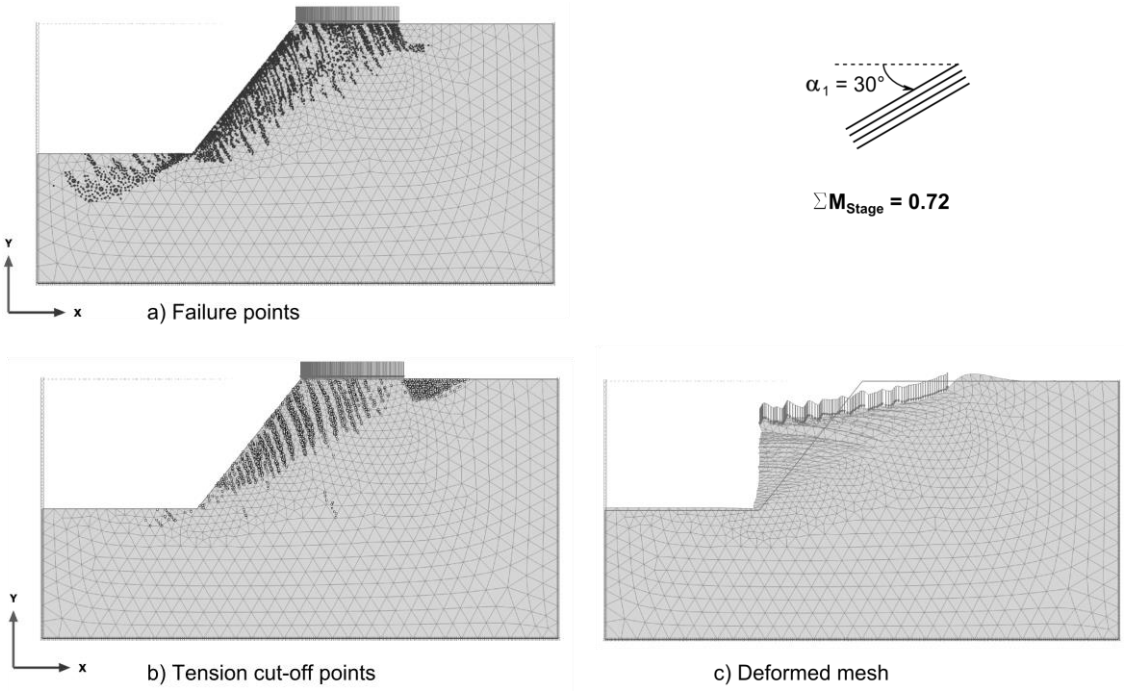

Fig. 21 Applied distributed load: plastic points (left column) and deformed mesh (right column) for α_1 = 30°, last calculation step, ΣM_{Stage} = 0.72

The development of the failure body is outlined in Fig. 22. It shows the plastic points history and the deformed mesh during phase 2 (load).

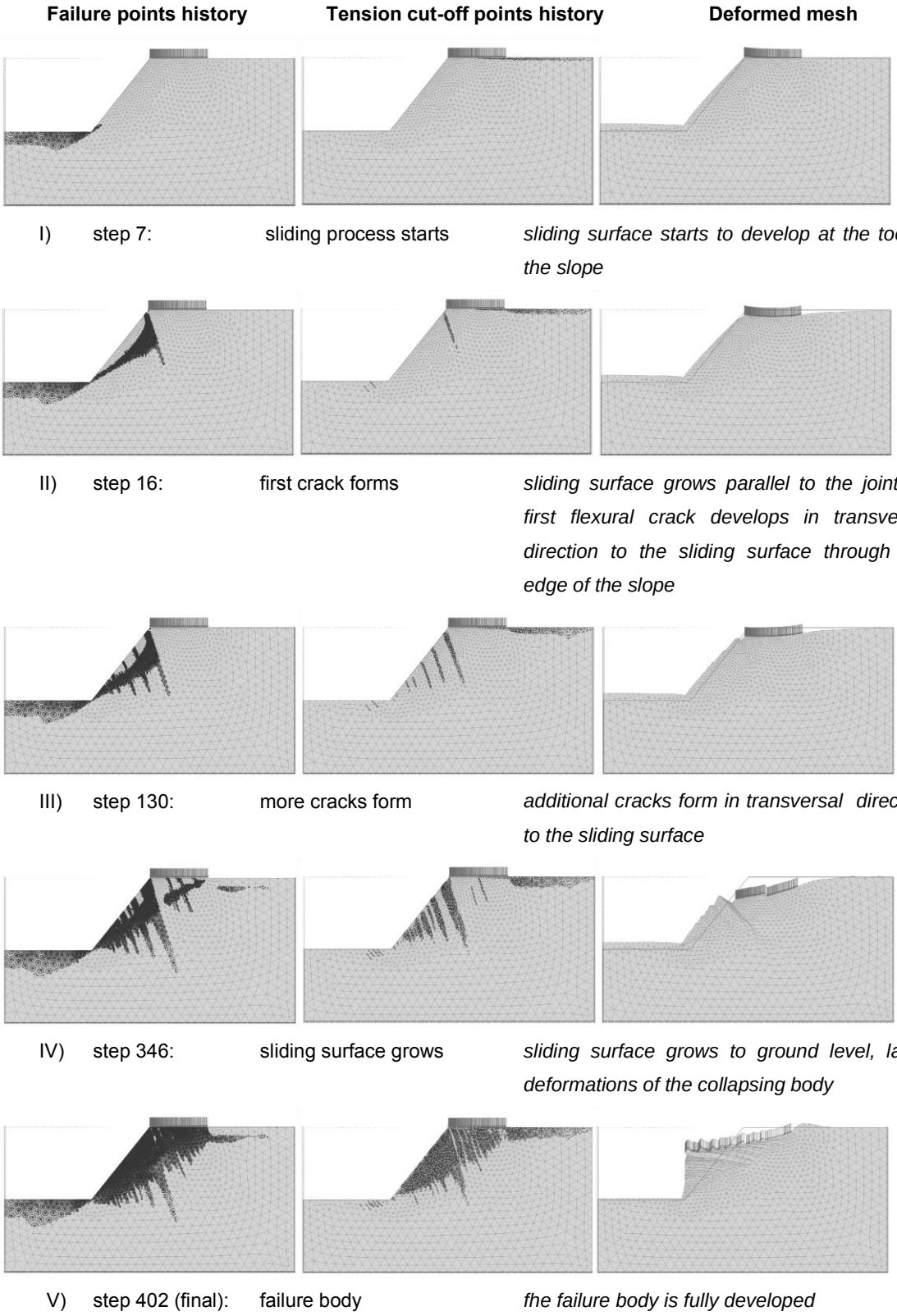

I) step 7: sliding process starts — *sliding surface starts to develop at the toe of the slope*

II) step 16: first crack forms — *sliding surface grows parallel to the jointing; first flexural crack develops in transversal direction to the sliding surface through the edge of the slope*

III) step 130: more cracks form — *additional cracks form in transversal direction to the sliding surface*

IV) step 346: sliding surface grows — *sliding surface grows to ground level, large deformations of the collapsing body*

V) step 402 (final): failure body — *fhe failure body is fully developed*

Fig. 22 Development of the failure body due to an applied load, $\alpha_1 = 30°$, $\Sigma M_{Stage} = 0.72$

4.3.2 Flexural toppling

According to Goodman and Bray (1976) flexural toppling occurs in hard rock slopes with well-developed steeply dipping discontinuities.

Equations (15) and (16) together with Fig. 23 describe the kinematic condition for flexural toppling (Graz University of Technology, Institute for Rock Mechanics and Tunneling 2007).

$$\alpha + \beta + 90° - \varphi = 180° \tag{15}$$

With α [°] … inclination angle of the joint ($\neq \alpha_1$)

β [°] … inclination angle of the slope

φ [°] … friction angle of the joint

Therefore toppling occurs for:

$$\beta > (90° - \alpha) + \varphi \tag{16}$$

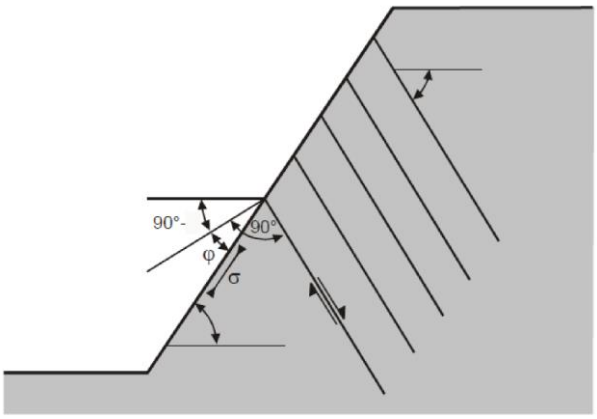

Fig. 23 Kinematic conditions for rock toppling (Graz University of Technology, Institute for Rock Mechanics and Tunneling 2007)

Goricki (1999) performed numerous base friction tests to analyze the behaviour of jointed rock structures. Fig. 24 shows the toppling procedure starting from the initial state (Fig. 24 - 1). After some time the joints start to open and a fracture due to flexural toppling develops transversely to the joints, creating multiple sliding surfaces (Fig. 24 - 4).

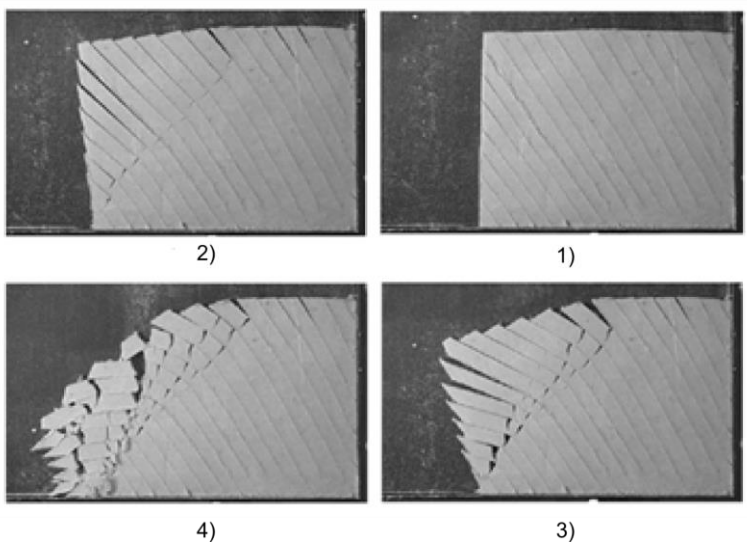

Fig. 24 Model test: Failure states in case of flexural toppling (Goricki, 1999)

In the following sections this type of failure is discussed by the example of a dip angle α_1 = 120°, which corresponds to α = 60°. The slope has an inclination angle of β = 50° and the friction angle of the joints is φ = 20°. According to (16) it holds:

$$50 > (90 - 60) + 20 \qquad (17)$$

$$50 = 50$$

The slope is in a limit equilibrium state.

4.3.2.1 *Failure due to a φ/c-Reduction*

The FEM-simulation consists of three calculation phases: initial phase; excavation phase; and safety calculation (φ/c-Reduction, see also 4.3.1.2), as listed in Tab. 8.

Tab. 8 Calculation phases for safety analysis of a JR slope

Phase nr.	**Phase ID**	**Calculation type**	**Loading type**
Phase 0	Initial phase	K_0-procedure	Staged construction
Phase 1	Excavation	Plastic	Staged construction
Phase 2	Safety	φ/c-reduction	Incremental multipliers

Note: Arc length control is switched *off* in phase 0 and phase 1 (see section 4.5 Arc length control)

The toppling process described above is well visualized in Fig. 25. . Tensile stresses develop in the upper part of the structure, marked by tension cut-off points (Fig. 25 b). This indicates an “opening” of the joints due to a flexural movement towards the

excavation. This deflection leads to a fracture in transverse direction to the joints, as indicated by failure and tension cut-off points (Fig. 25 a and b). The sliding surface of a quadrilateral failure body is formed as shown by a dashed line in Fig. 25 c. The factor of safety computes to 2.14.

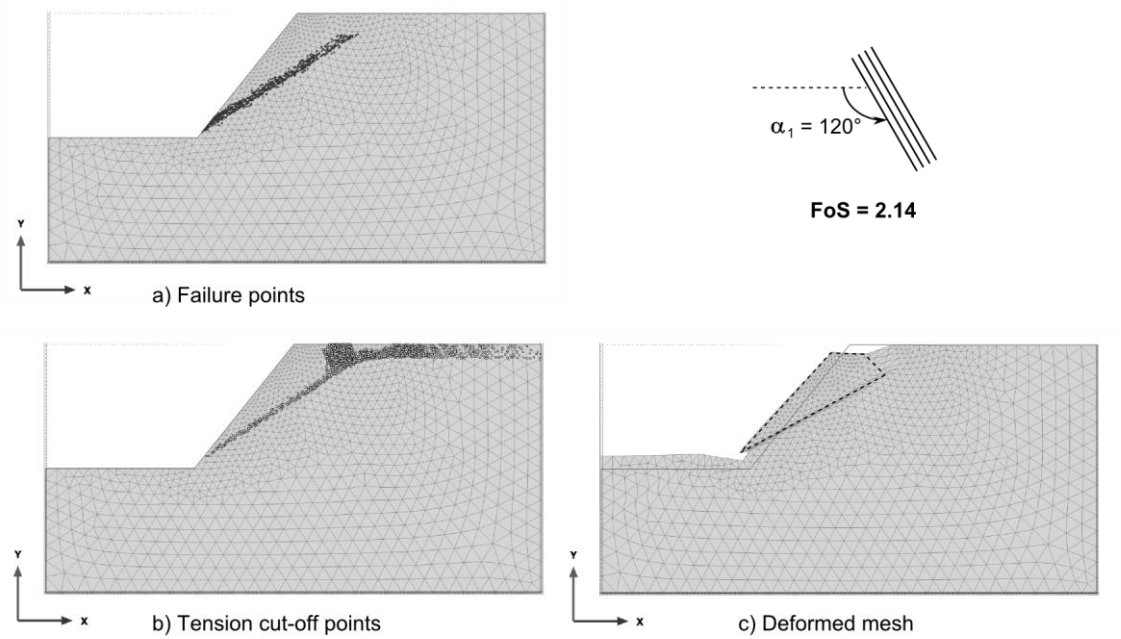

Fig. 25 Plastic points and deformed mesh of a cut slope after φ/c-reduction α_1 = 120°, FoS = 2.14

4.3.2.2 *Failure due to a uniform vertical load*

For the same structure as in the previous section (α_1 = 120°) the collapse of the cut slope is induced by a uniform vertical load q_y instead of a safety calculation.

The output is shown in Fig. 26. Examining the distribution of plastic points, the characteristic behaviour of JR material experiencing a vertical loading can be observed. Failure and plastic points develop transversal to the jointing due to deflection. The concentration of tension cut-off points (Fig. 26 b) indicates an “opening” of joints as a consequence to toppling close to the ground level and at the edge of the slope. A small triangular body develops at the edge of the slope, moving nearly perpendicular to the joint inclination along the created sliding surface towards the excavation.

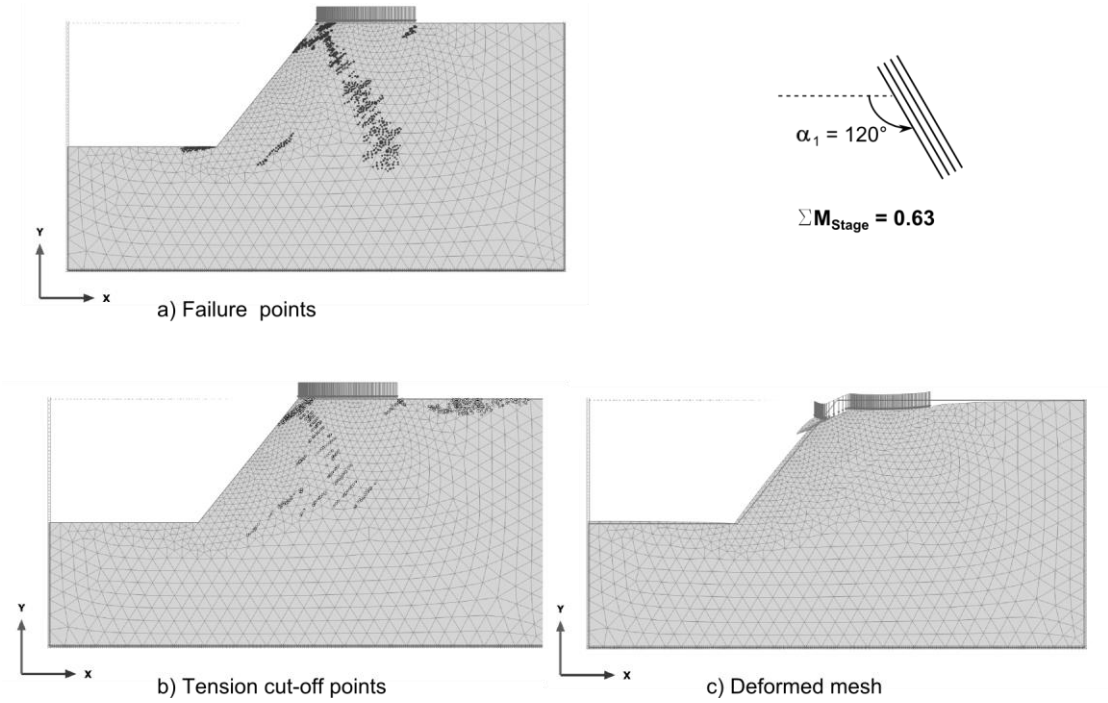

Fig. 26 Plastic points and deformed mesh of a cut slope after failure due to an applied load, α_1 = 120°, M_{Stage} = 0.63

Inspecting the plastic points history, the failure mechanism is visualized even better. The presence of numerous cracks transversal to the jointing can be observed. Plastic sliding and tensile stresses parallel to the jointing indicate an opening of the joint at the end of the load q_y. Referring to Fig. 24, this behaviour is characteristic of flexural toppling.

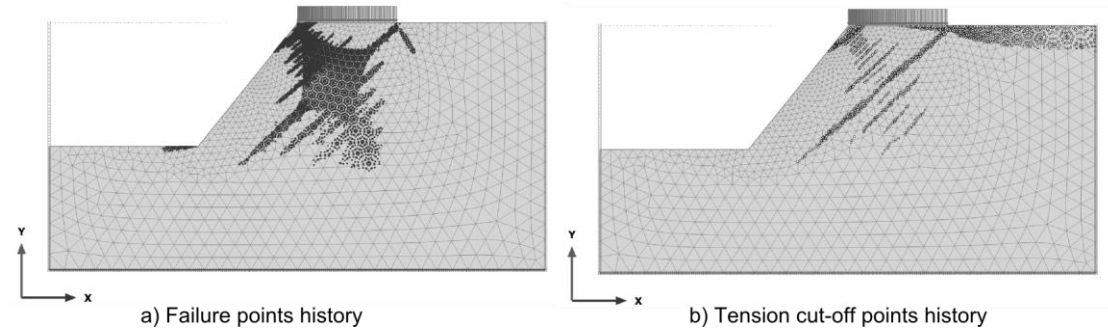

Fig. 27 Plastic points history of a cut slope after failure due to an applied load, α_1 = 120°, ΣM_{Stage} = 0.63

4.3.3 Behaviour of JR slopes with shallow dip angles

The behaviour of a structure which fulfils none of the criterions for parallel sliding and flexural toppling is analyzed on the example of a slope with a dip angle α_1 = 150°. The slope inclination angle is β = 50°, therefore, the jointing is in transverse direction and parallel sliding along the joints will not take place. According to (16) toppling does not occur for a dip angle of α_1 = 150° ≙ α = 30°

$$50 > (90 - 30) + 20 \tag{18}$$

$$50 < 80$$

The kinematic condition for toppling is not fulfilled and the structure is stable against toppling.

Fig. 28 shows the output of a φ/c-reduction for α_1 = 150°. The plot does not allow any reliable assumptions for a plausible failure mechanism after performing a φ/c-reduction. The high value of 61.6 for the computed FoS also indicates that a safety calculation is not appropriate in this case. The reason is that the failure cannot develop because the intact rock mass is considered elastic and the failure of joints is kinematically impossible.

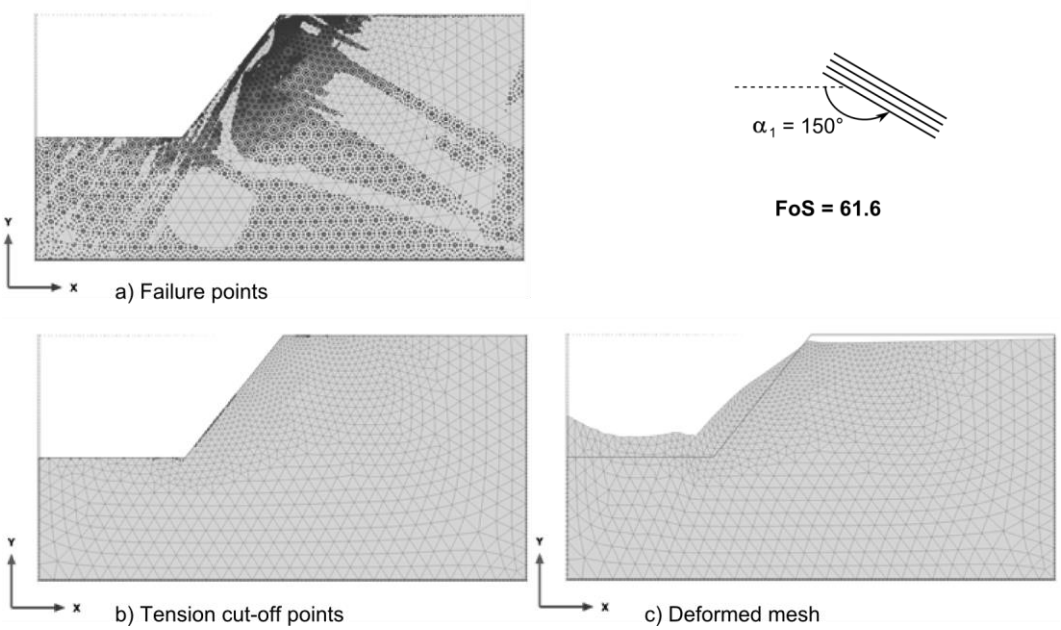

Fig. 28 Plastic points and deformed mesh after a safety calculation, α_1 = 150°, FoS=61.6

Triggering failure by means of an additional load leads to results that are easier to interpret. Fig. 29 shows the plastic points and the deformed mesh of the structure due to an applied load. The structure is in equilibrium (ΣM_{Stage} = 1.00), but a fracture in transverse direction to the jointing can be observed.

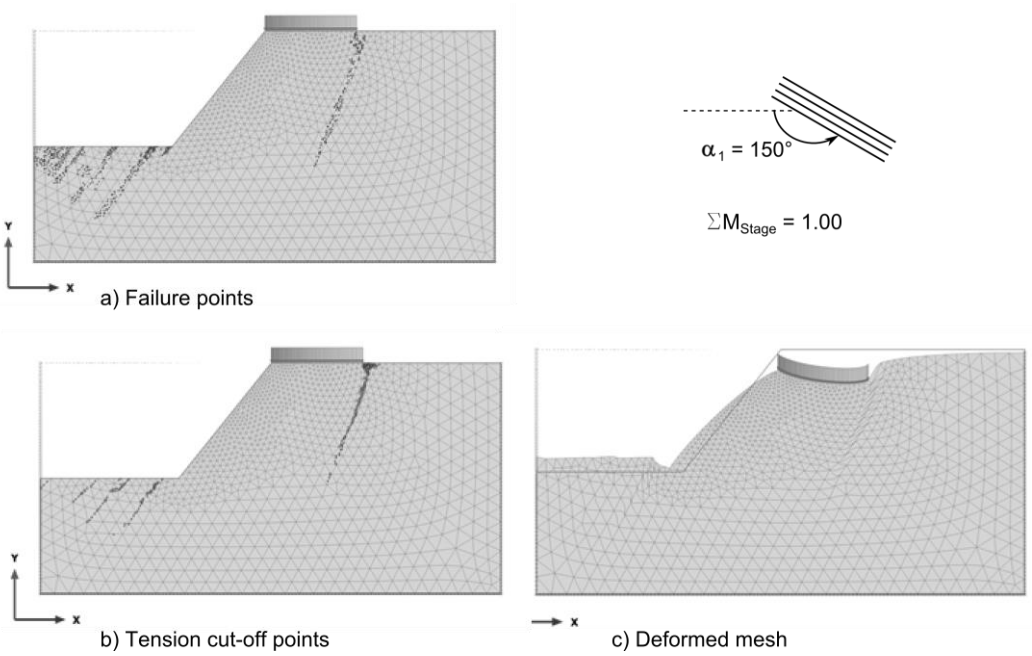

Fig. 29 Plastic points and deformed mesh due to an applied load, α_1 = 150°, ΣM_{Stage}=1.00

4.3.4 Influence of anisotropy

The material set from the previous section is changed so as to simulate transversal anisotropic behaviour. The stratification direction is represented by sliding plane 1 (α_1 = 30°). The stiffness perpendicular to the stratification direction is reduced compared to the general stiffness. It holds:

$$\nu_1 = \nu_2 = 0.3\ [-] \tag{19}$$

$$E_2 = \frac{E_1}{2.5} \tag{20}$$

$$= \frac{20000}{2.5} = 8000\ kN/m^2$$

In the present example the shear modulus G_2 is explicitly defined as being the mean value of G_{E1} and G_{E2}:

$$G_{E1} = \frac{E_1}{2(1+\nu)} \tag{21}$$

$$= \frac{20000}{2 * (1+0.3)} = 7692\ kN/m^2$$

$$G_{E2} = \frac{E_2}{2(1+\nu)} \tag{22}$$

$$= \frac{8000}{2 * (1+0.3)} = 3077\ kN/m^2$$

$$G_2 = \frac{G_{E1} + G_{E2}}{2} \tag{23}$$

$$= \frac{7692 + 3076}{2} = 5385\ kN/m^2$$

All material parameters are listed in Tab. 9.

Tab. 9 Material properties of a cut slope with anisotropic material behaviour

Identification	**Unit**	**Value**
Identification	[-]	JR
Material model	[-]	Jointed rock
Drainage type	[-]	Non-porous
γ	[kN/m³]	20.00
E_1	[kN/m²]	20000.00
ν_1	[-]	0.30
E_2	[kN/m²]	8000.00
ν_2	[-]	0.30
G_2	[kN/m²]	5385.00
Number of planes	[-]	1 plane
c_{ref}	[kN/m²]	100.00
φ	[°]	20.00
ψ	[°]	0.00
α_1(alpha 1)	[°]	varies
Tension cut-off	[-]	Yes
σ_t	[kN/m²]	0.00
K_0 determination	[-]	Manual
$K_{0,x}$	[-]	1.00

Quantitative results for stresses and deformations are valid for successfully performed calculation phases only (i.e. phase 0 and 1). Tab. 10 and Tab. 11 compare the results for maximum values of displacements and total principal stresses at the end of the excavation process between isotropic (i.e. $E_1 = E_2 = 20000$ kN/m²) and anisotropic material.

Tab. 10 Maximum displacements after the excavation phase: isotropic vs. anisotropic material

	Isotropic [m]	**Anisotropic [m]**
$\|u_{max}\|$	0.494	0.908

In this case the change in the elastic properties causes a difference of 0.414 m, which corresponds to an increase in deformations of 84 %.

Tab. 11 Total principal stresses after the excavation phase: isotropic vs. anisotropic material

	Isotropic [kN/m²]		**Anisotropic [kN/m²]**	
σ_{max}	48	(tension)	130	(tension)
σ_{min}	-1601	(compression)	-1375	(compression)

The failure criterion according to Coulomb, and the corresponding parameters remain the same; hence there is no change in the failure mechanism itself (Tab. 12).

Tab. 12 Total load level in the last calculation step (failure): isotropic vs. anisotropic material

	Isotropic [-]	**Anisotropic [-]**
ΣM_{Stage}	0.72	0.72

4.3.5 Influence of dilatancy

The dilatancy angle ψ is used in the plastic potential function *g* and determines the plastic volume expansion due to shearing (Brinkgreve et al. 2014a). By introducing the dilatancy angle $\psi = 10°$ the overall stability in increased. This condition is represented by ΣM_{Stage}:

Tab. 13 Total load level in the last calculation step (failure): differing dilatancy angle

	$\psi = 0°$ [-]	**$\psi = 10°$ [-]**
ΣM_{Stage}	0.72	0.92

Fig. 30 a shows the plastic points for $\psi = 0°$ and Fig. 30 b shows those for $\psi = 10°$. The dip angle is equal to 30°. It is visualized that by introducing a dilatancy angle, the majority of the stress points that show plastic behaviour fulfill the failure criterion according to Coulomb and fewer points reach the tension cut-off criterion.

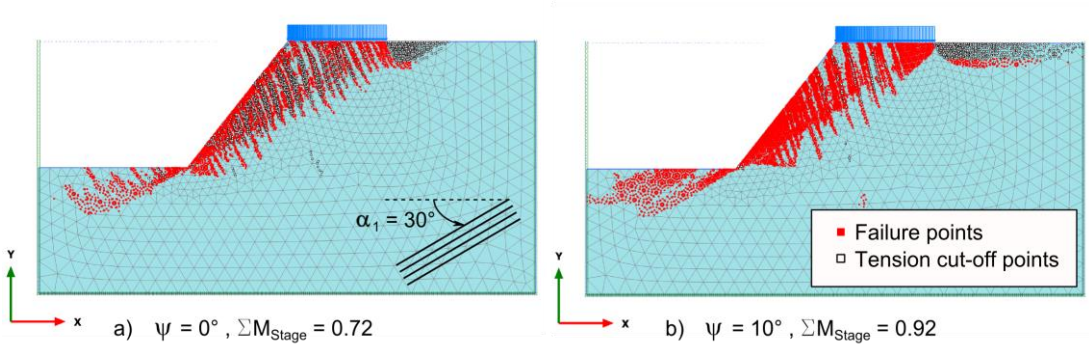

Fig. 30 Plastic points for differing dilatancy angles, $\alpha_1 = 30°$

4.3.6 General remarks on the use of φ/c-reduction with JR material

The *FoS* is displayed as a function of displacement |*u*| for all investigated dip angles in the two graphs below. Fig. 31 shows plausible results for the cases for which the governing failure types are *sliding of a rock body* and *flexural toppling*. Fig. 32 presents the results for shallow dip angles. The values increase exponentially, which does not represent a valid result. This leads to the conclusion that a safety calculation is not suitable for failure analyses of structures with shallow dip angles that will not collapse due do plastic shearing of the joints.

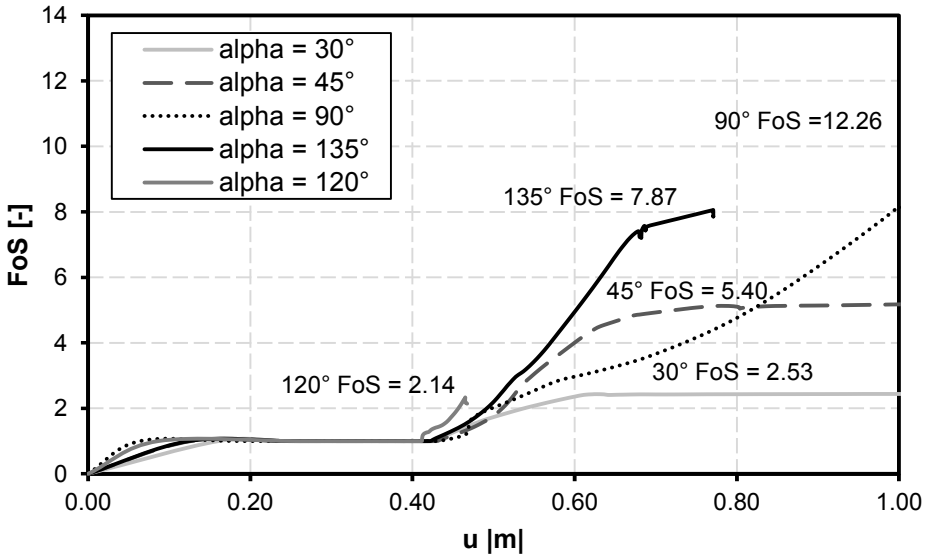

Fig. 31 FoS for $\alpha_1 = 30° / 45° / 90° / 120° / 135°$

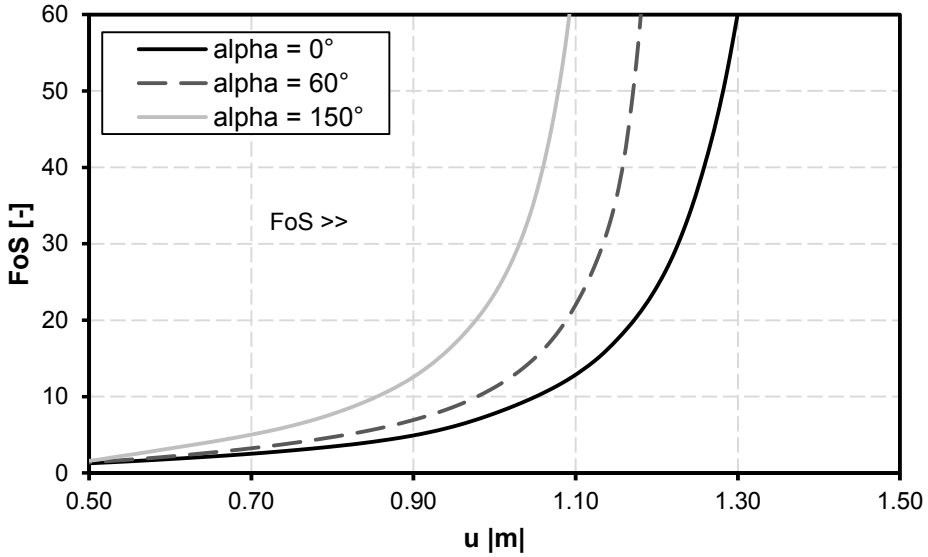

Fig. 32 FoS for α_1= 150° / 60° / 0°

4.4 Comparative simulations with the Iso-JRMC model (Bonnier & Brinkgreve 2013)

The Jointed Rock model with overall Mohr-Coulomb failure criterion (Iso-JRMC) is a user defined soil model for PLAXIS that combines the Jointed Rock model and the Mohr Coulomb model. As in the JR model plasticity can occur in up to 3 directions (planes) with the controlling parameters cohesion c, friction angle φ, dilatancy angle ψ and tensile strength σ_t. In the Iso-JRMC model the Mohr-Coulomb criterion is true for all other directions, based on principal stresses in "random" directions (parameters c_{MC}, φ_{MC}, ψ_{MC} and σ_{MC}) Hence, it is possible that failure occurs along the sliding planes as well as in the intact rock, which is not possible for JR material. To visualize the effect of this difference in the material behaviour, the output of two JR and Iso-JRMC simulations is compared.

4.4.1 Material properties and calculation phases

The output of slopes with a dip angles of α_1 = 30° and α_1 = 60° and material properties according to Tab. 14 is compared.

The simulations consist of three calculation phases (Tab. 15). The failure analysis is based on a φ/c-reduction.

Tab. 14 Material properties for JR and Iso-JRMC material

Identification	Unit	JR	Iso-JRMC
Material model	[-]	Jointed rock	User-defined
Drainage type	[-]	Non-porous	Non-porous
γ	[kN/m³]	20.00	20.00
E_1	[kN/m²]	20000.00	-
ν_1	[-]	0.30	0.3
E_2	[kN/m²]	20000.00	-
ν_2	[-]	0.30	-
G_2	[kN/m²]	7692.00	7692.00
c_{MC}	[kN/m²]	-	1000.00
φ_{MC}	[°]	-	37
ψ_{MC}	[°]	-	0
σ_{MC}	[kN/m²]	-	0
Number of planes	[-]	1 plane	1 plane
c_{ref}	[kN/m²]	100.00	100.00
φ	[°]	20	20
ψ	[°]	0	0
α_1	[°]	60 / 30	60 / 30
Tension cut-off	[-]	Yes	Yes
σ_t	[kN/m²]	0.00	0.00
K_0 determination	[-]	Manual	Manual
$K_{0,x}$	[-]	1.00	1.00

Tab. 15 Calculation phases of comparative simulations (JR and JRMC)

Phase nr.	Phase ID	Calculation type	Loading type
Phase 0	Initial phase	K0-procedure	Staged construction
Phase 1	Excavation	Plastic	Staged construction
Phase 2	Safety	φ/c-reduction	Incremental multipliers

4.4.2 Output

Fig. 33 presents the comparison of the incremental displacements for the Iso-JRMC (a) and JR (b) models after a φ/c-reduction for a dip angle of $\alpha_1 = 30°$. In both cases a sliding plane parallel to the dip direction and according to the kinematic freedom of the system is developed but the triangular failure body is more explicitly formed in case of JR material.

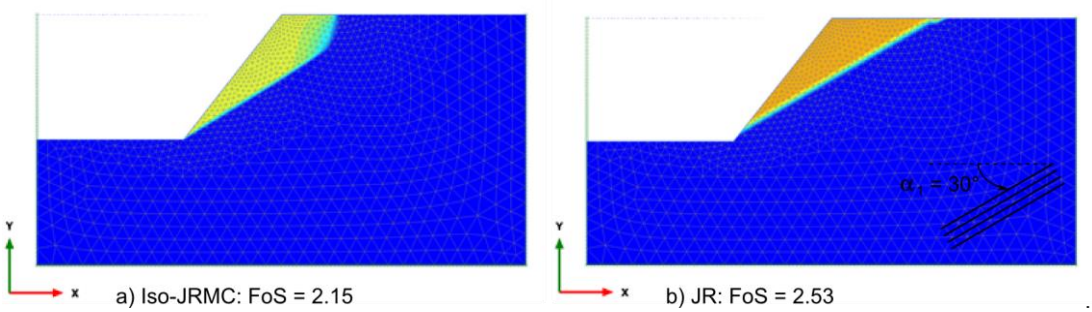

Fig. 33 Incremental displacements: JR and JRMC, α_1 = 30°

The plastic points of the two systems are compared in Fig. 34. The blue marks in Fig. 34 a represent the plastic sliding in JR material, the grey marks indicate a tension cut-off in MC material in the upper part of the failure body. The plastic points in JR material are plotted in Fig. 34 b. The factor of safety is higher for the JR material but as discussed in section 4.3.2.1, in case of JR material the FoS is highly dependent on the mesh coarseness.

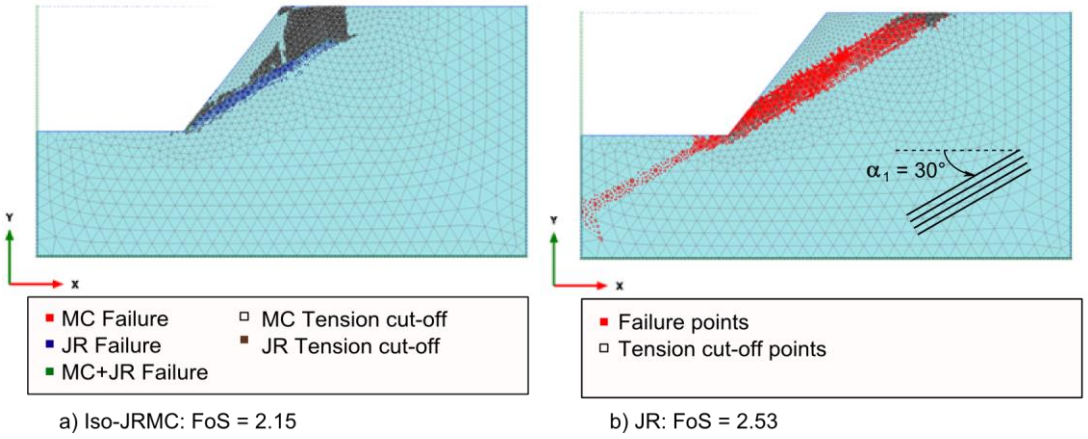

Fig. 34 Plastic points: JR and JRMC: α_1 = 30°

The difference between the two material models becomes more visible for a structure which is kinematically stable, as it is the case for a dip angle of α_1 = 60°, which is presented below. The Iso-JRMC structure (Fig. 35 a) shows a plausible failure body with two sliding surfaces parallel to the jointing until excavation level and a concave sliding surface below the slope toe. The structure is stable and has a computed FoS of 7.1.

Fig. 35 b does not allow a meaningful assumption of the failure body but it can be concluded that there is plastic shearing in the sliding planes. Also, the FoS cannot be taken as a valid solution (see also 4.3.6).

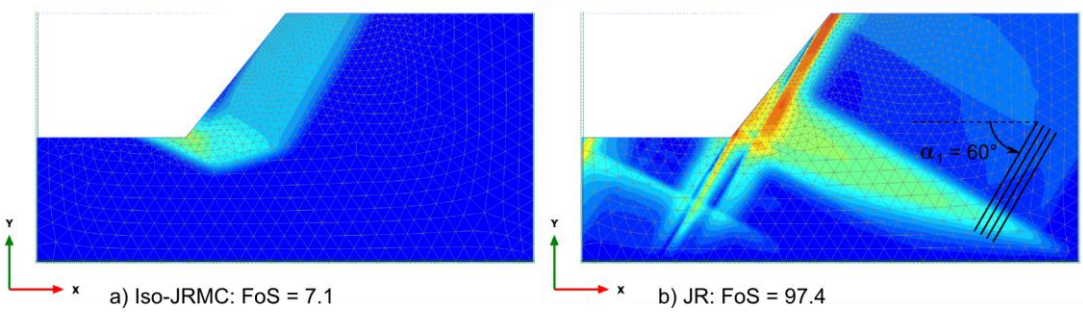

Fig. 35 Incremental displacements: JR and JRMC, α_1 = 60°

Fig. 36 shows plots of the plastic points in the two structures. Again, the failure body is better visible in the Iso-JRMC structure (Fig. 36 a). The different shadings indicate in which part of the material shear or tensile failure occurs. The Jointed Rock material fails at the blue stress points and red points indicate the failure of the Mohr Coulomb material, which represents the intact rock. The green failure points at the lower part of the failure body represent a transitional area where there is plastic sliding in jointed rock as well as in the intact material and there are tension cut-off points in the MC material close to the ground level.

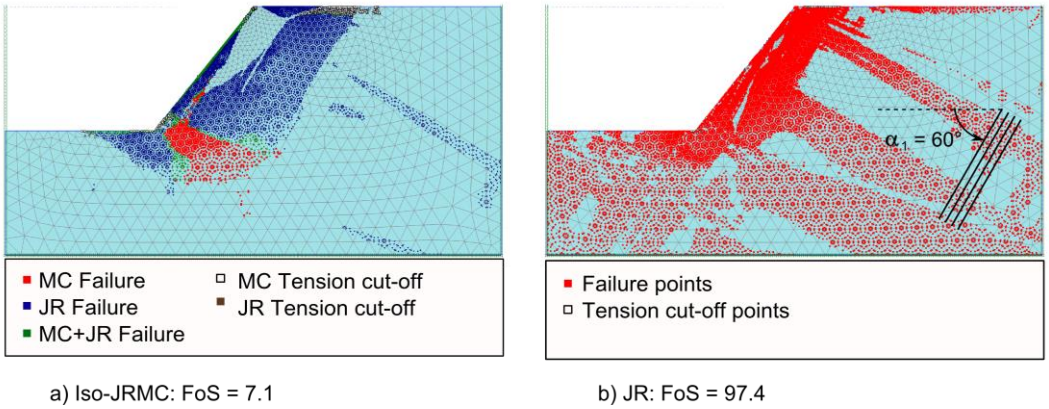

Fig. 36 Plastic points: JR and JRMC: α_1 = 60°

The results of the comparative simulation emphasize the fact that in the JR model only the sliding planes fail, since they have limited shear strength according to Coulomb's criterion, but not the intact rock which is defined as being elastic material.

4.5 Arc length control

Arc length control is a solution technique for nonlinear calculations in the finite element method. Instead of calculating a solution within a certain load increment, the code computes a solution within a certain arc length. The load advancement is governed by the predefined number of loading and unloading steps. In general the application of this

solution technique may lead to a decrease in computing time. In PLAXIS 2D AE this technique is active by default and can be switched off by the user.

Fig. 37 shows a comparison between the resulting ΣM_{Stage} (failure load) for arc length control switched *on* and *off,* respectively. The failure is induced by applying a uniform load on the upper horizontal boundary of the slope (see sections 4.3.1.3 and 4.3.2.2). In all cases except for α_1 = -30° (no failure at all) the reached ΣM_{Stage} is significantly higher when the application is deactivated. The arc length control application detects a local failure, such as cracking, which might not be the final failure mechanism (Fig. 38). Consequently the use of this solution technique might lead to a severe misinterpretation of the results when investigating failure mechanisms for structures containing JR materials.

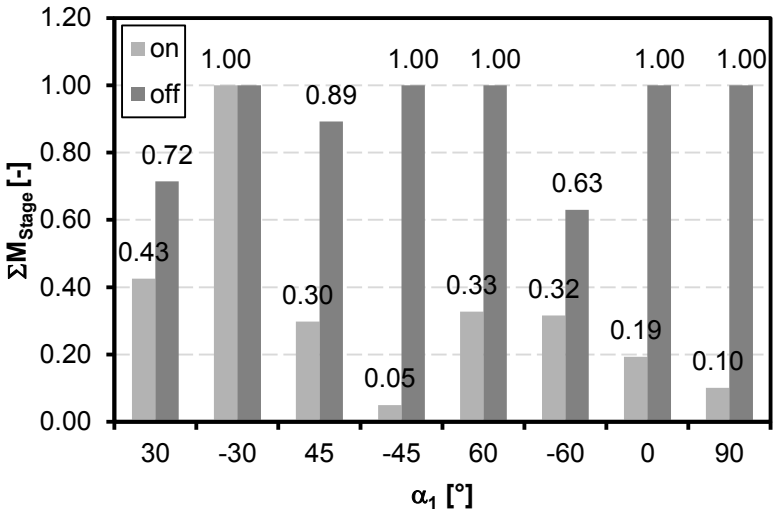

Fig. 37 Comparison between ΣM_{Stage} reached for arc length control *on/off* (2810 elements)

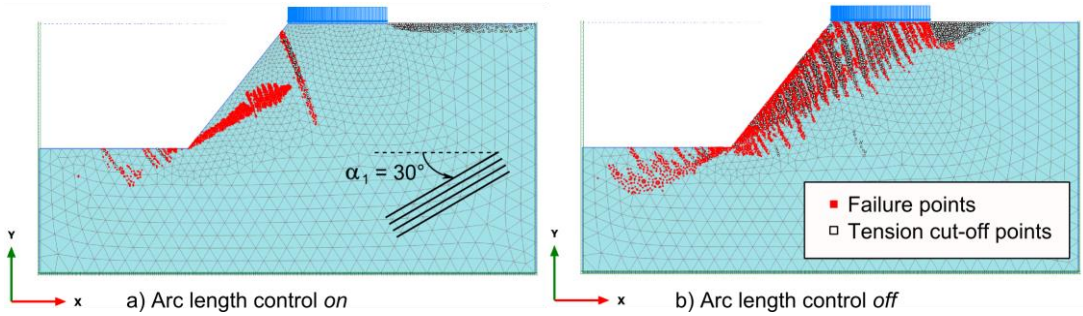

Fig. 38 Comparison between plastic point distributions at failure for *arc length control on / off*

PLAXIS 2D AE offers the possibility to increase the maximum number of unloading steps manually. To eliminate the possibility of a premature failure it is still recommended not to use the arc length control technique.

Based on these findings it is recommended to change the *Arc length control* to *off* in the numerical control parameter section when working with the JR material model, especially if failure mechanisms are to be investigated, which are initiated by increasing the load and not by a φ/c-reduction.

General remark: For *Safety* calculations *arc length control* is to be switched *on* (Brinkgreve et al. 2014b).

4.6 Conclusions

The failure mechanisms of a cut slope consisting of JR material is investigated by inducing a collapse of the structure by means of a φ/c-reduction and a uniform vertical load. Depending on the kinematic conditions, failure mechanisms such as parallel sliding of a body or flexural toppling occur. For other failure mechanisms a φ/c-reduction is not very meaningful since it does not lead to valid results for the failure body or the *FoS*.

Comparative simulations prove that there may be a significant difference whether the intact rock material is defined to be elastic material (PLAXIS JR material model) or Mohr-Coulomb material (user-defined Iso-JRMC material model). In the JR material failure will occur in the sliding planes only, whereas in the Iso-JRMC model failure can occur in both the intact rock as well as in the sliding planes.The significance of the influence of the material for the intact rock depends on the geometry and the boundary conditions of the analyzed problem and has to be investigated independently for specific problems.

Calculations have been performed with and without the use of the *arc length control*. The results lead to the conclusion that when working with the JR material model it is recommended to deactivate the *arc length control* to eliminate the possibility of a premature failure.

5 Tunnel excavation

This chapter presents a full face tunnel excavation problem in Jointed Rock material. The findings from the previous chapters are applied to this problem and the new calculation results are interpreted to make valid assumptions for basic tunnel excavation problems.

The influence of the dip angle α_1 as well as the coefficient of earth pressure at rest K_0 on the failure mechanism is investigated. In a first set of simulations the behaviour of the JR mass after the excavation process without any tunnel support is analyzed and in a second set of simulations the forces acting on a concrete lining are discussed.

5.1 Geometry and mesh coarseness

The cross section has the diameter d_1 of 10.19 m in x-direction and the diameter d_2 of 9.72 m in y-direction. It has an overburden of 29.15 m, which corresponds to $3d_2$. The lower model boundary has a distance of 19.44 m ($2d_2$) from the tunnel invert which results in a total height h of 58.29 m. To ensure that the generated mesh does not influence the structure's behaviour during the simulation, the total width b of the model is $15d_1$ = 152.80 m. The geometries are shown in Fig. 39.

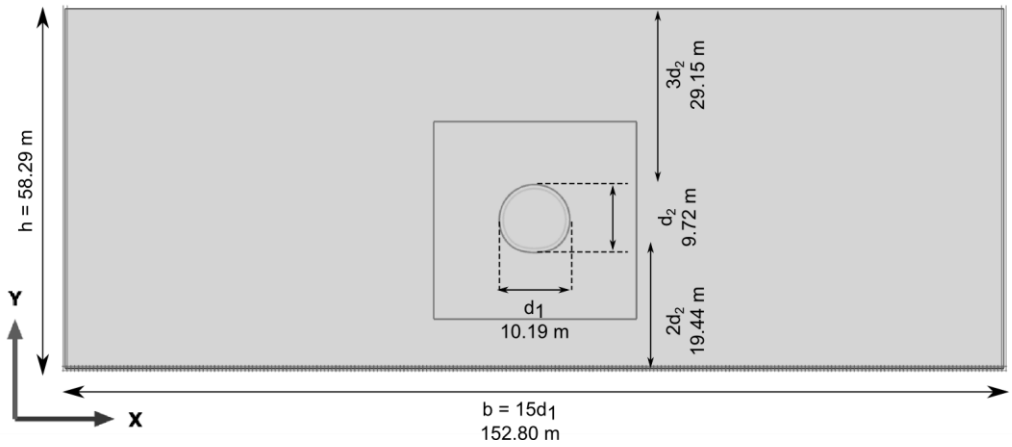

Fig. 39 Geometry of the tunnel excavation problem

The FEM model is a plane strain problem, consisting of 6570 15-noded elements. The mesh is refined within a square of 33 x 33 m around the tunnel cross section (Fig. 40).

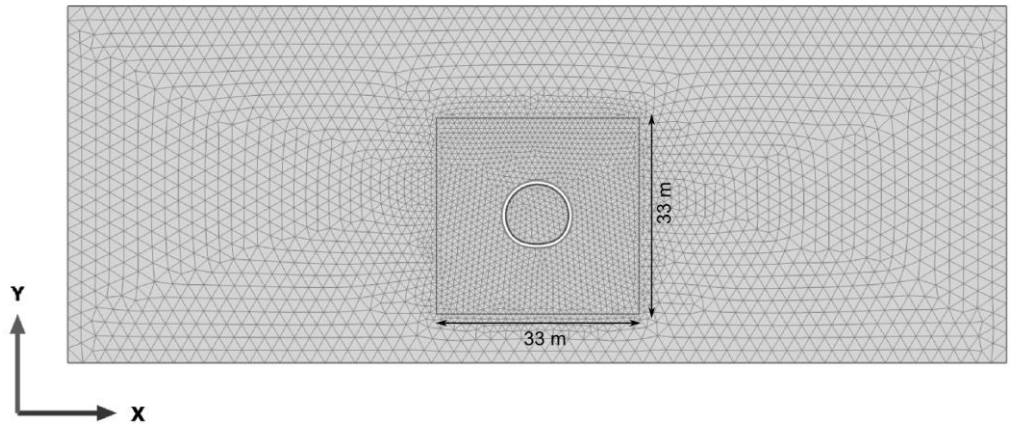

Fig. 40 FEM mesh of the tunnel excavation problem: 6570 15-noded elements

5.2 Material properties

The JR mass is defined to show isotropic behaviour and there is one set of sliding planes present (i.e. n = 1). The user-defined material properties for the JR material set are listed in Tab. 16. To simulate the behaviour of JR material with different joint geometries in a tunnel excavation process, the analyses are run with horizontal, vertical and inclined sliding planes:

$$\alpha_1 = 0°/\ 30°/\ 45°/\ 60°/\ 90°$$

The initial stress state is calculated by the K_0-procedure and the influence of different values for the coefficient of earth pressure at rest is investigated.

To analyze the behaviour of a collapsing JR structure, the strength properties of the sliding planes are defined such that failure occurs in absence of supporting structures after the excavation process for all investigated dip angles. This leads to comparable results.

Tab. 16 Material properties of the JR material in the tunnel excavation problem

Identification	Unit	Value
Identification		JR
Material model		Jointed rock
Drainage type		Non-porous
γ	[kN/m³]	25.00
E_1	[kN/m²]	$2.0*10^6$
ν_1	[-]	0.2
E_2	[kN/m²]	$2.0*10^6$
ν_2	[-]	0.2
G_2	[kN/m²]	$8.33*10^5$
Number of planes	[-]	1 plane
c_{ref}	[kN/m²]	0.000
φ	[°]	20.000
ψ	[°]	0.000
α_1	[°]	0 / 30 / 45 / 60 / 90
Tension cut-off	[-]	Yes
σ_t	[kN/m²]	0.000
K_0 determination	[-]	Manual
$K_{0,x}$	[-]	0.5 / 1.0 / 1.5

5.3 Failure analysis of the tunnel excavation

When discussing failure mechanisms of an excavation in a jointed rock mass, two basic failure types are noted (Graz University of Technology, Institute for Rock Mechanics and Tunneling 2007):

- **Failure of a rock fragment:**
  The degree of jointing, joint geometry, number and orientation of the major joint families in respect to each other and to the excavation are influencing parameters for the failure of a rock fragment.

- **Stress induced failure**
  Due to a redistribution of stresses and changes of the boundary conditions after an excavation process, the rock material experiences an overstress with collapse as a possible consequence. This type of failure does mainly occur in continuous and homogenous rock mass.

To numerically investigate the failure of the tunnel excavation, the FEM analysis is simulated by performing a staged construction consisting of two calculation phases according to Tab. 17. The initial state is computed by the K_0-procedure and the excavation is executed as a full face excavation in a single calculation step of the type *plastic* in phase 1. Failure occurs after the excavation process due to low strength parameters of the JR material. No support structures are being installed.

Tab. 17 Calculation phases of the tunnel excavation

Phase nr.	**Phase ID**	**Type**
Phase 0	Initial phase	K_0-procedure
Phase 1	Excavation	Plastic

Note: Arc length control is switched *off* in all phases (see section 4.5 Arc length control).

5.3.1 Influence of α_1 on the failure mechanism

To gain knowledge about the basic behaviour of a tunnel excavation in JR material, the influence of the dip angle α_1 is investigated in a first step. For this purpose a symmetric initial stress state is defined, i.e. $K_0 = 1.0$.

Goricki (1999) performed numerous base friction model tests to investigate the influence of continuous and parallel jointing on excavations. Fig. 41 shows a failure sequence of an excavation in horizontally jointed rock mass ($\alpha_1 = 0°$). The failure starts at the crown, is then propagated layer-wise in upwards direction and tapers off until a layer showing sufficient strength properties is reached. The joint acts as a boundary of the created excavation.

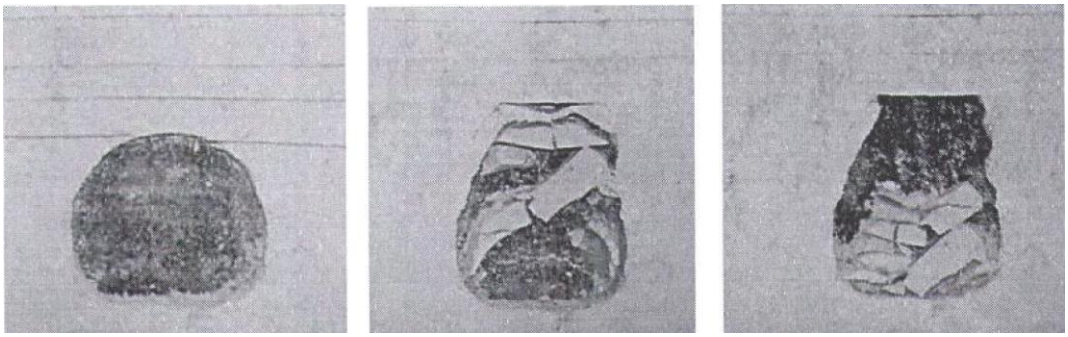

Fig. 41 Base friction model test of an excavation in horizontally jointed rock mass (Goricki 1999)

This behaviour is also visible in the calculation output of the numerical simulation with JR material. The deformed mesh and the corresponding failure points history of the tunnel excavation in JR mass with α_1 = 0° is plotted in Fig. 42. In contrast to the model test, there is no discrete joint that acts as a boundary for the failure body. As visualized by the failure points history, the plastic points form an isosceles triangle. The inclined sliding surfaces grow in upwards direction until they intersect and the failure body is fully developed. The excavation also leads to a heave of the invert, where a similar but less developed failure body can be observed. Additionally to the triangular body a sliding plane tangential to original crown and invert and parallel to the jointing develops.

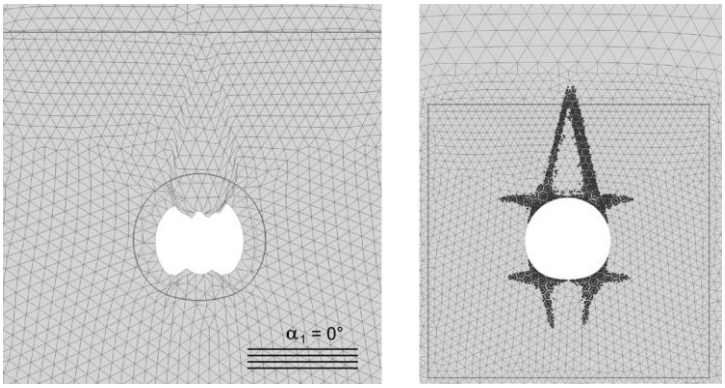

Fig. 42 Deformed FEM mesh and failure points history of an excavation in horizontally jointed rock mass, K_0 = 1.0

The failure points histories for JR masses with α_1 = 0° / 30° / 60° / 90° are plotted in Fig. 43. The failure body rotates according to the dip angle: the axis through the vertex of an isosceles triangle is perpendicular to the sliding plane.

With increasing inclination of the dip angle the total load level of the structure increases. Tangential to the excavation and parallel to the dip angle sliding planes develop on opposite sides of the excavation. The tension cut-off points history for α_1 = 0° is shown in Fig. 44. They occur together with plastic points on the crown and the invert. The shape and the location of the failure can be interpreted as a buckling of the rock layers due to the excavation and the absence of support structures.

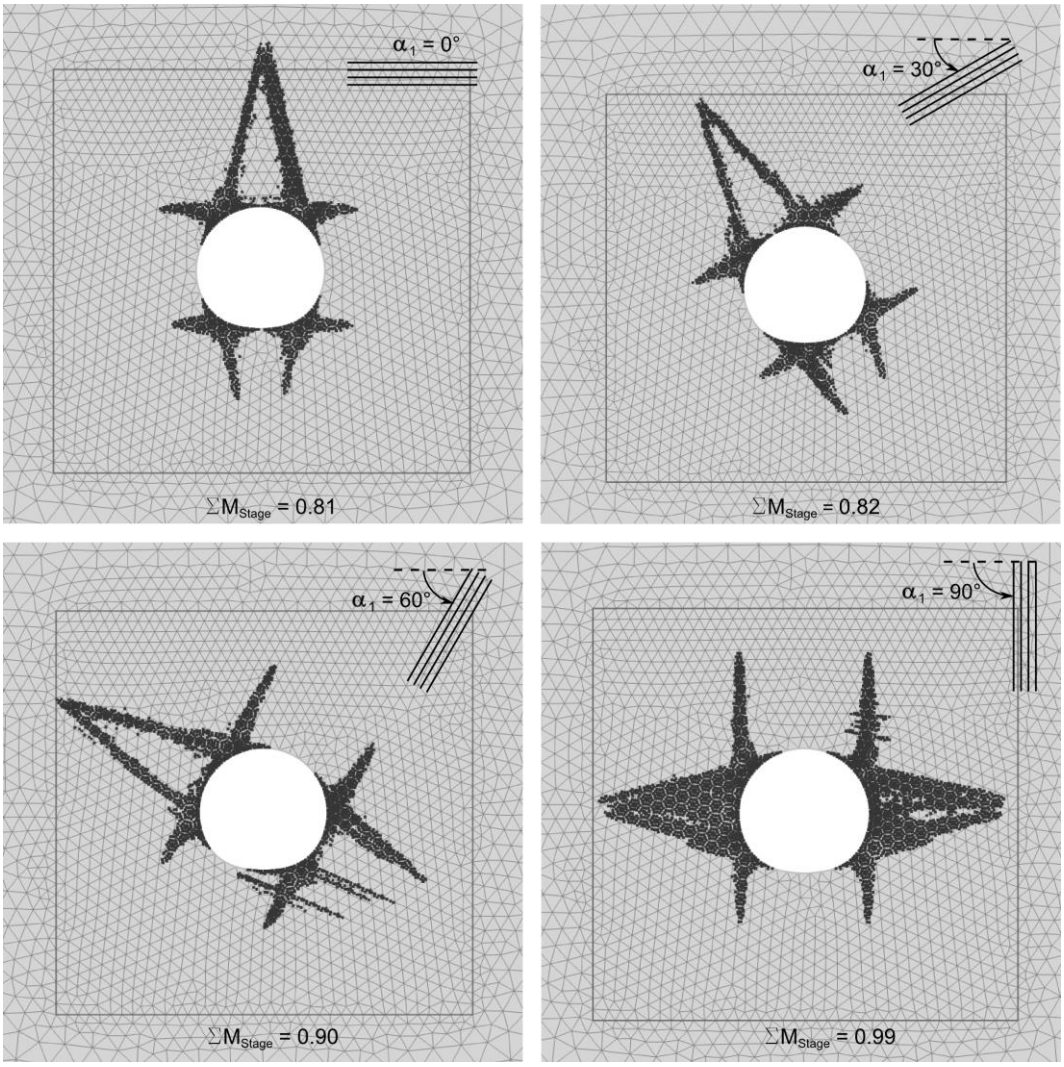

Fig. 43 Failure points history for varying α_1, K_0 = 1.0

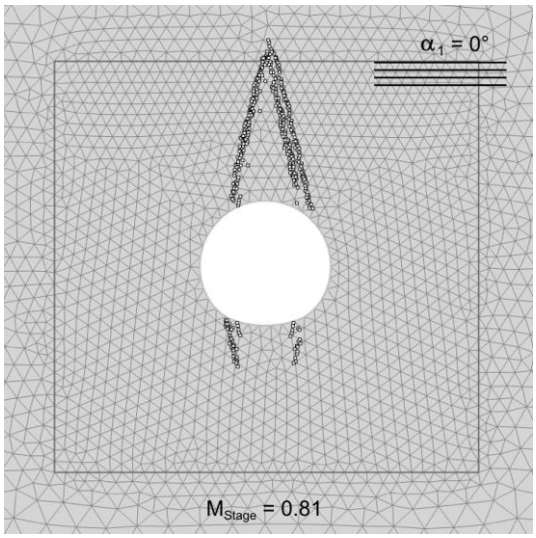

Fig. 44 Tension cut-off points history, α_1 = 0°, K_0 = 1.0, M_{Stage} = 0.81

5.3.2 Influence of K_0

The behaviour of a rock mass after an excavation process is highly influenced by the initial stress state of the material, governed by the ratio between horizontal and vertical initial stress (K_0). To investigate how this factor influences a JR material, it is varied as follows:

$$K_0 = 0.5 / 1.0 / 1.5$$

The influence of K_0 on the failure is best visualized by the failure points history (Fig. 45). The increase in side pressure leads to more significantly developed sliding surfaces along the sliding plane defined by the dip angle α_1, whereas the primary failure body on the crown of the excavation, respectively perpendicular to the jointing, remains the same. In case of horizontal jointing (i.e. $\alpha_1 = 0°$) there is no significant change in the total load level at failure (ΣM_{Stage}), whereas for the case $\alpha_1 = 30°$ and $K_0 = 1.5$ the reached load level is significantly lower. A sliding surface transversal to the jointing develops and failure is reached at $\Sigma M_{Stage} = 0.37$. It is visualized that the coefficient of earth pressure at rest may have destabilizing as well as stabilizing effects, depending on the dip angle of the joints. The most significant influence of the side pressure with respect to the failure mechanism can be observed for $\alpha_1 = 90°$. In case of a low K_0, the rock body above the excavation slides into the opening, while the stability (represented by ΣM_{Stage}) increases with growing K_0, finally resulting in a totally different failure mechanism (Fig. 45, bottom row).

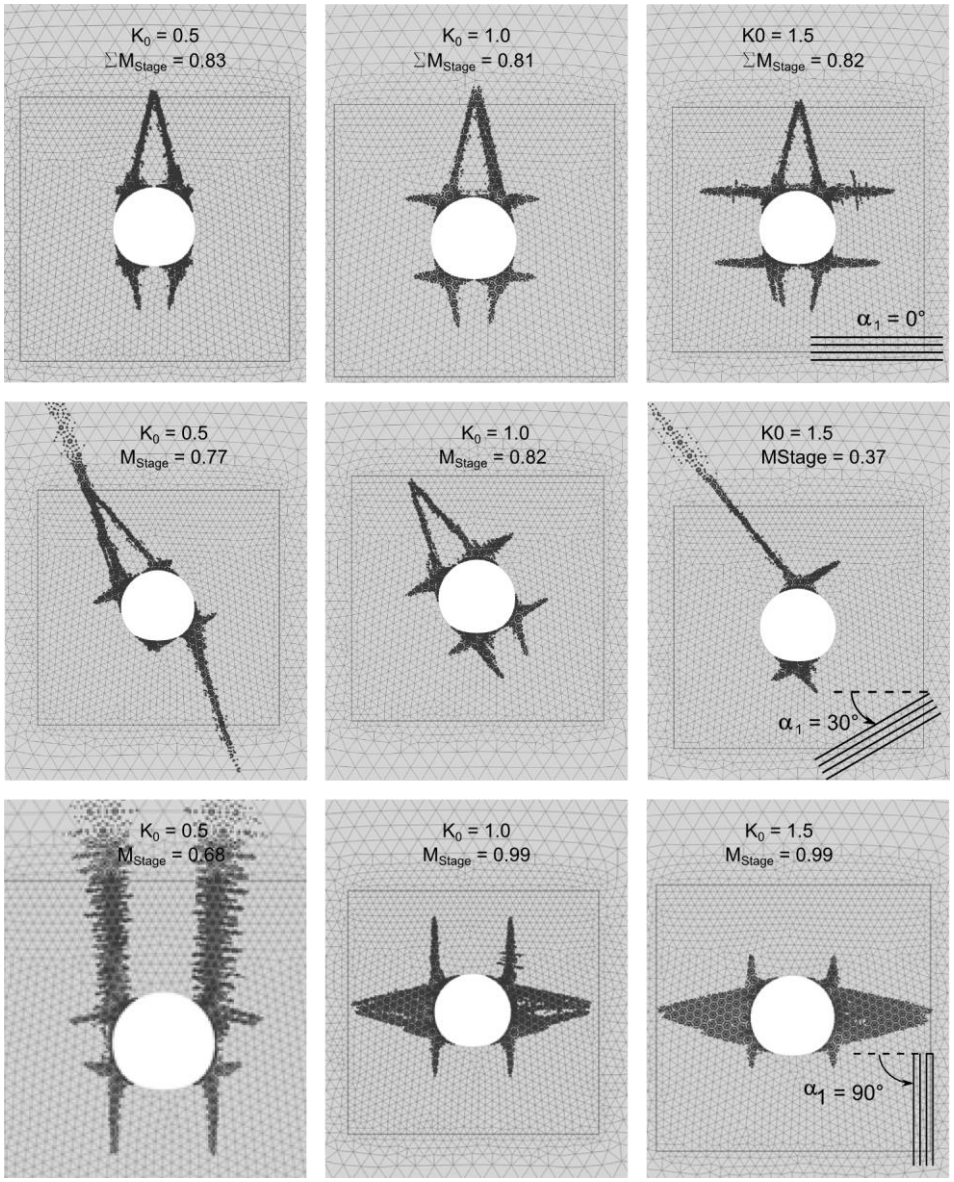

Fig. 45 Failure points history, $\alpha_1 = 0°$ (first row) , $\alpha_1 = 30°$ (middle row) and $\alpha_1 = 90°$(bottom row), varying K_0

The influence of the combination of dip angle α_1 and the coefficient of earth pressure at rest K_0 is shown in Fig. 46. In general, the reached load level ΣM_{Stage} varies to a small extend only. Significantly lower values can be observed for $\alpha_1 = 30°$ $K_0 = 1.5$ and $\alpha_1 = 90°$ $K_0 = 0.5$, leading to the assumption that the stabilizing or destabilizing effects of K_0 depend on the dip angle of the joints.

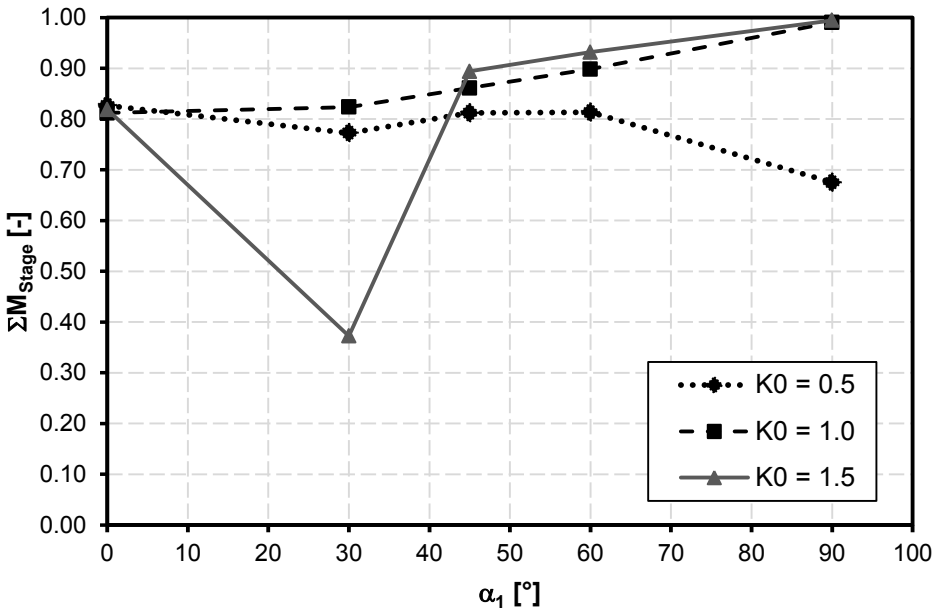

Fig. 46 Total load level ΣM_{Stage} for increasing α_1 and varying K_0

5.3.3 Influence of dilatancy

The dilatancy angle ψ is used in the plastic potential function g and determines the plastic volume expansion due to shearing (Brinkgreve et al. 2014a). By introducing the dilatancy angle ψ = 10° the overall stability is increased. This condition is represented by a slightly higher value for ΣM_{Stage}:

Tab. 18 Total load level in the last calculation step (failure): differing dilatancy angle

	ψ = 0° [-]	**ψ = 10° [-]**
ΣM_{Stage}	0.81	0.87

Fig. 47 a shows the plastic points for ψ = 0° and Fig. 47 b shows those for ψ = 10°. The dip angle is equal to 45°. By introducing a dilatancy angle the majority of the stress points that show plastic behaviour fulfill the failure criterion according to Coulomb, and fewer points reach the tension cut-off criterion. On the left hand side of the tunnel excavation, the sliding surface parallel to the jointing is further developed in case of ψ = 10°.

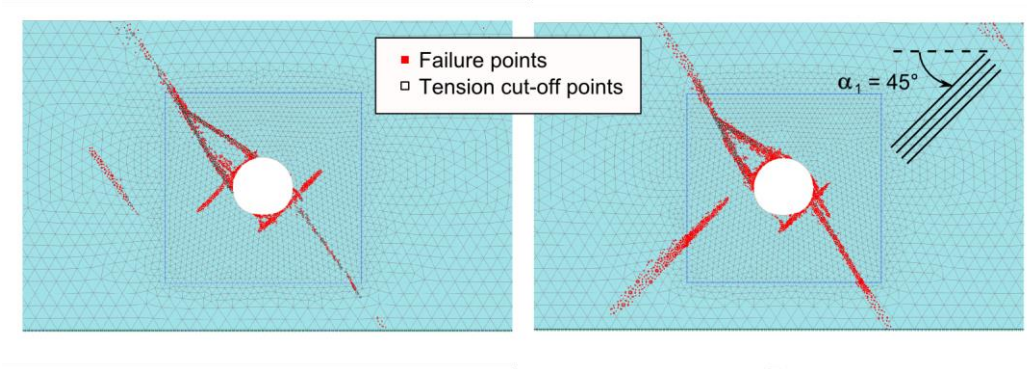

Fig. 47 Plastic points for differing dilatancy angles, α_1=45°

5.3.4 φ/c-Reduction

The failure type due to a φ/c-reduction for inclined jointing (α_1 = 60°) is investigated. The simulation consists of three calculation phases as listed in Tab. 19. To ensure equilibrium in all calculation phases, the strength properties of the sliding planes are increased to c = 50 kN/m² and φ = 27°.

Tab. 19 Calculation phases for safety analysis of a tunnel excavation in JR material

Phase nr.	Phase ID	Calculation type	Loading type
Phase 0	Initial phase	K_0-procedure	Staged construction
Phase 1	Excavation	Plastic	Staged construction
Phase 2	Safety	φ/c-reduction	Incremental multipliers

Note: Arc length control is switched *off* in phase 0 and phase 1 (see section 4.5 Arc length control)

The calculation output for α_1 = 60° is presented in Fig. 48. Two failure planes transversal to the sliding plane develop, resulting in a very similar failure mechanism as it was discussed in the previous analyses of failure due to the dead weight of the rock mass and the prescribed mechanical properties. The shape of the failure body and the location of the tension cut-off points indicate that the failure body “rips off” and intends to move towards the excavation (see also Fig. 41). The FoS computes to 1.64, which represents equilibrium. To increase the stability of the structure, support structures should be installed.

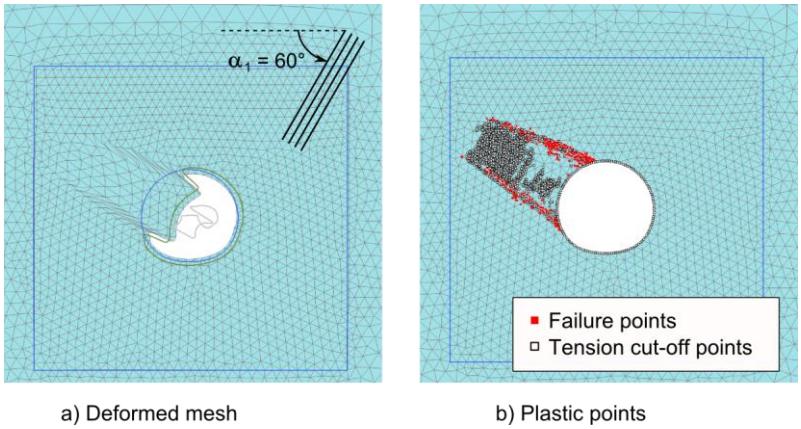

Fig. 48 Failure due to a φ/c-reduction, α_1=60°, FoS = 1.64

Fig. 49 presents the deformed mesh (a) and the plastic points (b) for a JR mass with vertical joints (c =10 kN/m², φ = 25°, α_1 = 90°) The FoS computes to 1.60. The graphics indicate that a rectangular mass above the excavation moves parallel to the jointing into the opening. In addition, the plastic points form isosceles triangles at the tunnel sidewalls, representing typical behaviour for RJ mass, as discussed in the previous sections.

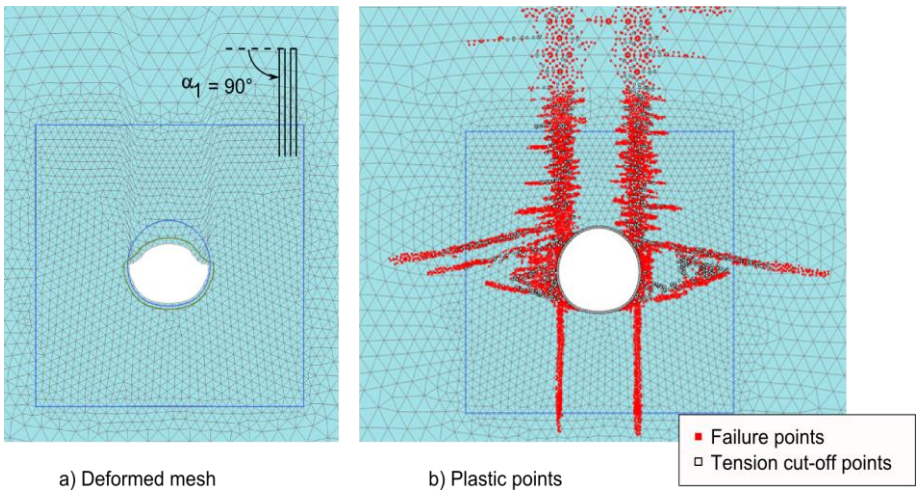

Fig. 49 Failure due to a φ/c-reduction, α_1=90°, FoS = 1.60

The graph in fig. 50 shows the development of the FoS as a function of the displacement for the tunnel excavations in JR material with vertical and inclined jointing. The value for the FoS does not stabilize with increasing displacement, which is an unfavorable situation for a φ/c-reduction. It can be concluded that for tunnel excavation problems the φ/c-reduction is a suitable approach only if qualitative failure analyses are performed (see also chapter 4.3.6).

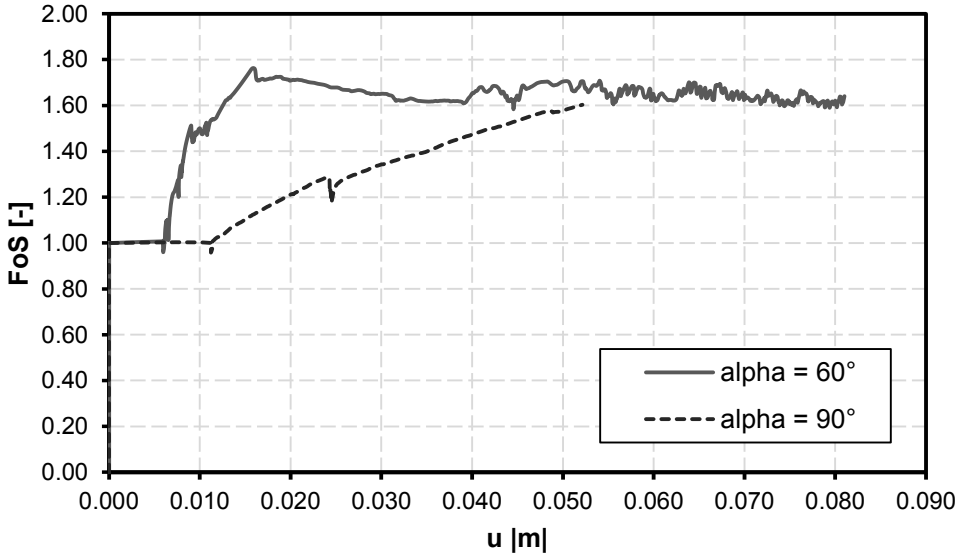

fig. 50 Factor of Safety FoS over displacement *u* for α_1 = 60°

5.3.5 Comparative simulations with the Iso-JRMC model

The tunnel excavation is performed using Iso-JRMC material (see 4.4) to investigate the influence of the use of Mohr-Coulomb material instead of elastic material for the intact rock. The calculation output is compared to the results of the simulation with JR material. The dip angles of the jointing are 30° and 90°, all material properties for both material sets are shown in Tab. 20.

Tab. 20 Material properties for JR and Iso-JRMC material

Identification	**Unit**	**JR**	**Iso-JRMC**
Material model	[-]	Jointed rock	User-defined
Drainage type	[-]	Non-porous	Non-porous
γ	[kN/m³]	20.00	25.00
E_1	[kN/m²]	$2.00*10^6$	-
ν_1	[-]	0.20	0.20
E_2	[kN/m²]	$2.00*10^6$	-
ν_2	[-]	0.20	-
G_2	[kN/m²]	$8.33*10^5$	$8.33*10^5$
c_{MC}	[kN/m²]	-	200
φ_{MC}	[°]	-	37
ψ_{MC}	[°]	-	0
σ_{MC}	[kN/m²]	-	0
Number of planes	[-]	1 plane	1 plane
c	[kN/m²]	0	0
φ	[°]	25	25
ψ	[°]	0	0
α_1	[°]	30 / 90	30 /90
Tension cut-off	[-]	Yes	Yes
σ_t	[kN/m²]	0.00	0.00
K_0 determination	[-]	Manual	Manual
$K_{0,x}$	[-]	0.5	0.5

The plastic points plotted in Fig. 51 show that changing the material does not lead to a significant difference in the failure load represented by ΣM_{Stage}, which results to 0.77 in both cases. While the location of the plastic points is almost identical in both plots their identification is different. Fig. 51 a indicates that there is plastic sliding as well as tension in the joints in case of elastic material for the intact rock. If the intact rock behaves as MC material there is plastic sliding in the joints as well as in the intact rock, indicated by blue and green points in Fig. 51 b. It can be concluded that the failure mechanism itself is not significantly influenced by the material of the intact rock but by the jointing. The failure can be categorized as failure of a rock segment in this case (in contrast to stress induced failure, see chapter 5.3).

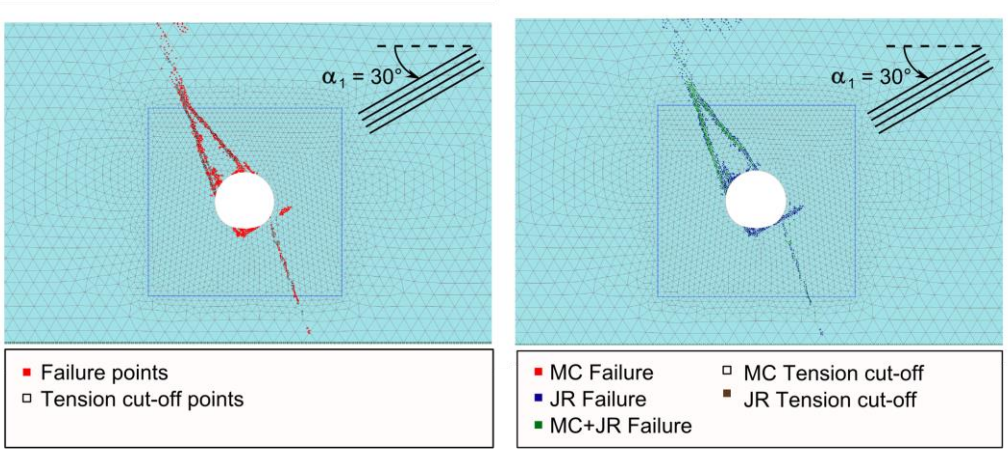

a) JR; ΣM_{Stage} = 0.77 b) Iso-JRMC; ΣM_{Stage} = 0.77

Fig. 51 Plastic points: JR and Iso-JRMC: α_1 = 30°

Similar behaviour can be observed for a vertical jointing (α_1 = 90°), as shown in Fig. 52.

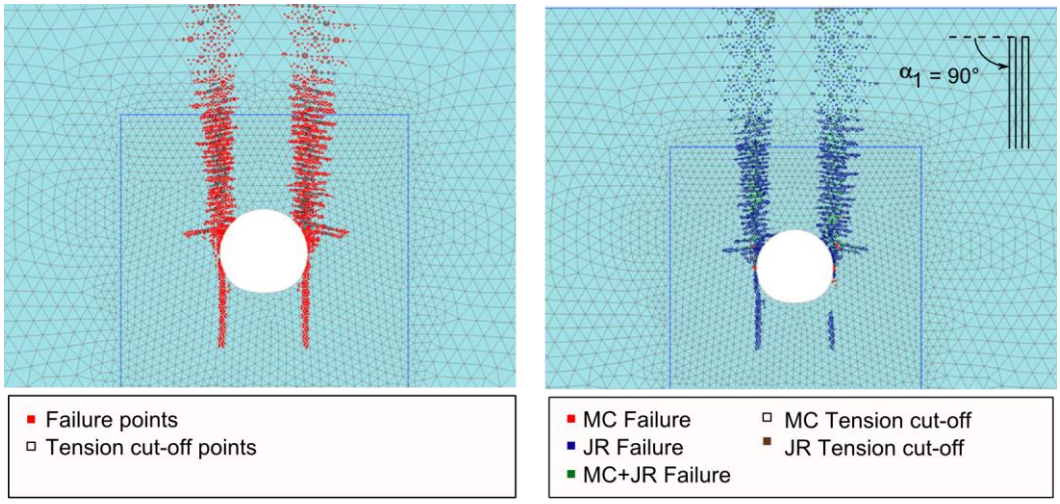

a) JR; ΣM_{Stage} = 0.68 b) Iso-JRMC; ΣM_{Stage} = 0.67

Fig. 52 Plastic points: JR and Iso-JRMC: α_1 = 90°

5.4 Forces on a concrete lining

A tunnel lining and an interface between support structure and adjacent JR material are installed in calculation phase 3. By introducing this third calculation phase, valid results for deformations and stresses for the situation right before failure are being generated and quantitative analyses can be carried out. To visualize the behaviour of the continuous material model for JR best, the tunnel excavation is performed in vertically jointed material (i.e. α_1 = 90°) and K_0 equal to 0.5. The calculation output is compared

to results of corresponding analytical calculations. The material properties of the concrete lining are listed in Tab. 21, the calculation phases of the simulation in Tab. 22.

Tab. 21 Material properties of the concrete lining

Identification	Unit	Value
Material type	[-]	elastic
EA_1	[kN/m]	$4.50*10^6$
EA_2	[kN/m]	$4.50*10^6$
EI	[kN/m²/m]	$3.38*10^4$
d	[m]	0.30
w	[kN/m/m]	0.00
ν	[-]	0.20

Tab. 22 Calculation phases of the excavation with support structures

Phase nr.	Phase ID	Calculation type	Loading type
Phase 0	Initial phase	K_0-procedure	Staged construction
Phase 1	Excavation	Plastic	Staged construction (ΣM_{Stage} = 0.67)
Phase 2	Lining	Plastic	Staged construction

Note: Arc length control is switched *off* in all phases (see section 4.5 Arc length control).

The total load level ΣM_{Stage} to be reached in the excavation phase is set to a decreased value of 0.67, which represents the moment right before the rock body collapses ($\Sigma M_{Stage,collapse}$ = 0.6751). In the subsequent calculation phase a tunnel lining which is modelled as a plate element and an interface between the supporting structure and the adjacent rock are activated. In the following, normal stresses on a cross section above the crown, as well as structural forces of the plate element are analyzed. Analyzing normal stresses on a cross section above the crown, as well as structural forces of the plate element shall provide evidence as, to whether the resulting forces correspond to the load that is acting on the structure due to the dead weight of the soil body, which rests on the support.

5.4.1 Normal stresses along a cross section

5.4.1.1 *Numerical simulation*

Fig. 53 shows the normal stresses acting on a cross section above the crown. The equivalent force computes to -3420 kN/m². This equivalent vertical force can be interpreted as the load acting in vertical direction on the support structure. By defining ΣM_{Stage} being 0.67, the moment just before the collapse of the structure is represented, signifying that the entire load of the rock body rests on the lining.

$\sigma_{n,max}$ = -175.6 kN/m²
$\sigma_{n,min}$ = -940.5 kN/m²
Equivalent force = - 3420 kN/m

Fig. 53 Normal stress on cross section above the crown, V = -3420 kN/m

The normal stress on the entire interface between the concrete lining and the adjacent rock mass is plotted in Fig. 54.

$\sigma_{n,max}$ = 0.0 kN/m²
$\sigma_{n,min}$ = - 455.5 kN/m²

$\sigma_{n,max}$ = -7.4 kN/m²
$\sigma_{n,min}$ = -172.4 kN/m²

Fig. 54 Normal stress σ_n on the interface between concrete lining and rock mass

5.4.1.2 *Analytical verification*

The numerical calculation output is compared to the results of a simplified analytical approach by means of a cross section above the crown. The weight force of the rectangular JR body *G* acts in negative y-direction on the cross-section, the supportive forces *R* represent the mobilized frictional forces from the horizontal side pressure force *H*. The static system is shown in Fig. 55.

Identification	Unit	Value
γ	[kN/m³]	25.00
h	[m]	29.15
d	[m]	10.19
K_0	[-]	0.50

$$G = \gamma * h * d \tag{24}$$

$$G = 25.00 * 29.15 * 10.19 = 7426\ kN/m$$

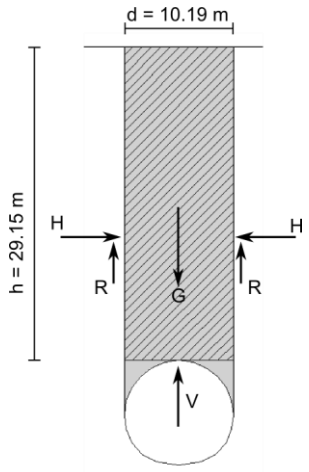

Fig. 55 Model for analytical approach

The initial horizontal stress σ_h:

$$\sigma_h = \gamma * h * K_0 \tag{25}$$

$$\sigma_h = 25 * 29.15 * 0.5 = 364.38\ kN/m^2$$

The resulting horizontal force *H*:

$$H = \frac{\sigma_h * h}{2} \tag{26}$$

$$H = \frac{364.38 * 29.15}{2} = 5311\ kN/m$$

The supportive friction forces result to:

$$R = H * \tan(\varphi) \tag{27}$$

$$R = 5311 * \tan(20) = 1933\ kN/m$$

Assuming equilibrium, the unknown vertical force *V* can now be calculated to:

$$V = G - 2R \tag{28}$$

$$V = 7426 - 2 * 1933 = 3560\ kN/m$$

The difference between the numerical and the analytical result is:

$$\Delta V = V_{analytical} - V_{numerical} \tag{29}$$

$$\Delta V = 3560 - 3420 = 140 \frac{kN}{m}$$

The difference between the analytical and numerical calculation results for the force acting on the crown computes to 4.1 %. Besides computational tolerances, the smaller value for the numerical result is due to the condition that the total reached load level is defined to be 0.67, indicating that the loading procedure is not fully completed and there is still a small load increment that is not yet acting on the structure.

This simple comparison points out that the continuous model without discrete joints and specified joint spacing behaves similar to a structure with two discrete joints.

5.4.2 Structural forces

Fig. 56 shows the axial force *N*, the shear force *Q* and the bending moment *M* of the concrete lining of a tunnel excavation in vertically jointed rock mass. The values of the structural forces at the crown are very small and the peak values in the shear force and the bending moment coincide with the location of the sliding (failure) surfaces that

develop due to plastic shearing. The deformed mesh and the plastic points of the excavation with a concrete lining are plotted in Fig. 57.

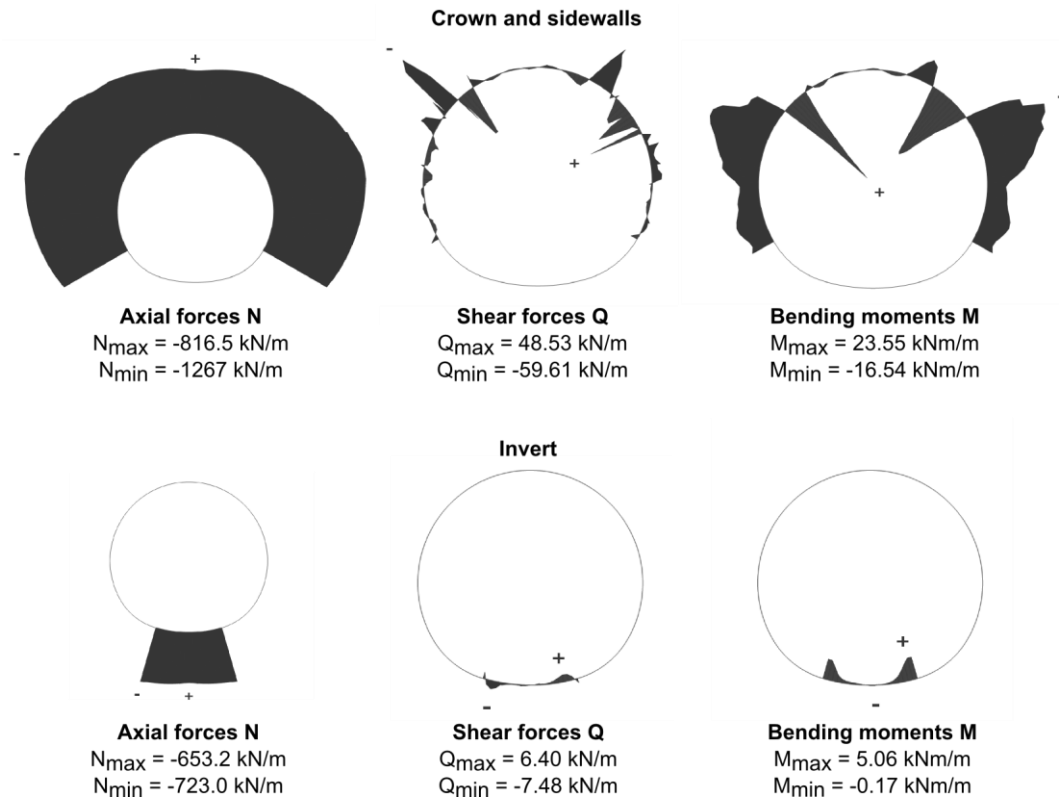

Fig. 56 Structural forces N, Q and M of the concrete lining

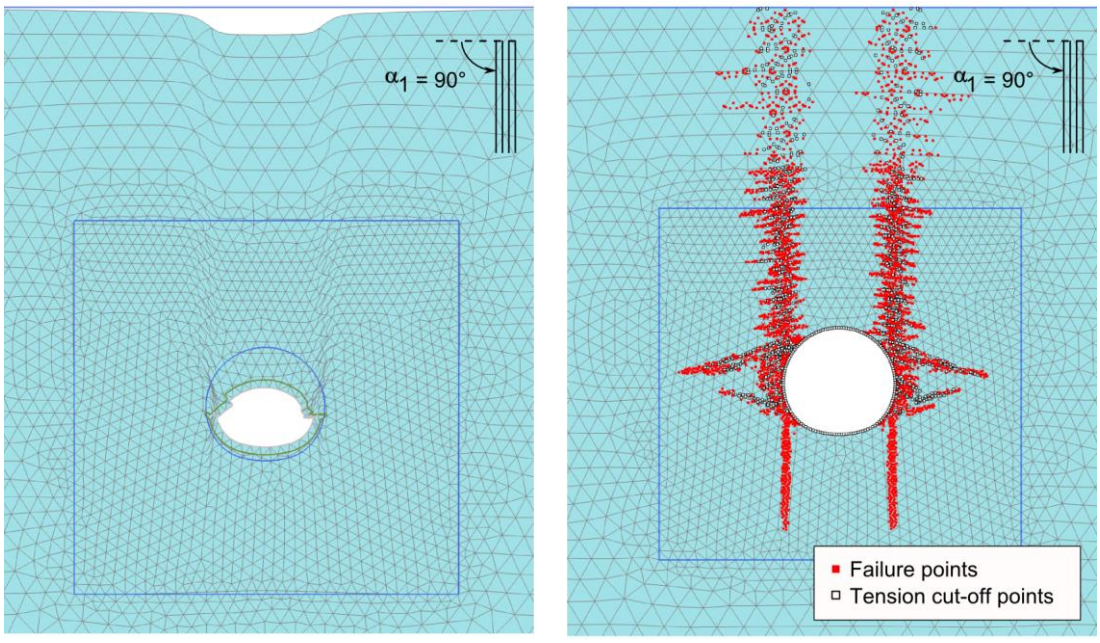

Fig. 57 Tunnel excavation with concrete lining: deformed mesh and plastic points, $\alpha_1 = 90°$

5.5 Conclusions

To gain knowledge about the general behaviour of JR material when performing a full face excavation a standard tunnel cross section without support structures is simulated.

The formation of a triangular failure body, or a single sliding surface in transverse direction to the jointing and the comparison of the numerical calculation output with model tests, show that the failure body is highly influenced by the dip angle of the parallel joints. The coefficient of earth pressure at rest K_0 might have small stabilizing or destabilizing effects on the structure, depending on the dip angle α_1. To qualitatively analyze the failure mechanism of a structure in equilibrium, a φ/c-reduction can be performed. Comparisons between the calculation output of simulations with elastic material for intact rock (JR) as well as with MC material for intact rock (iso-JRMC) show that failure occurs due to buckling of the rock layers, representing the failure of rock segments instead of failure due to stress redistributions as it might occur in intact and homogenous rock.

The comparison of analytical and numerical calculation results for a tunnel excavation in vertically jointed rock material shows that the continuous material behaves similar to a structure with discrete jointing.

6 Conclusion and Outlook

The present thesis investigated the general behaviour of structures consisting of Jointed Rock material, which represents a simplified material for a rock mass showing parallel joint sets or joint families that are not filled with fault gauge and have a small spacing compared to the overall dimensions of the structure.

Preliminary investigations on a cantilever show that the dip angle of the joints has a significant influence on the stress conditions and the failure mechanism of the structure, visualized by stress concentrations. By inducing a collapse of the structure by means of an applied uniform load, the influence of the dip angle is visualized by the formation of flexural cracks transversal to the jointing. When the failure body is fully developed, a sliding surface parallel to the jointing is formed. A cut slope is investigated in a subsequent chapter and the failure due to a φ/c-reduction and a uniform vertical load is analyzed. Typical failure mechanisms of jointed rock slopes such as parallel sliding or flexural toppling are very visible. Analyzing the failure due to a uniform vertical load shows that cracks develop in transverse direction to the jointing as a consequence of deflection. The simulation of a full face tunnel excavation in JR material shows that the failure mechanism is mainly influenced by the dip angle of the sliding planes. The rock layers fail due to flexural deflection visualized by plastic points transversal to the joint direction.

The results of a *safety* calculation are to be taken into account in qualitative analyses only. If the failure is not primarily related to the jointing and the kinematic boundary conditions, a φ/c-reduction is not suitable since only the sliding planes are assigned to underlie the MC-failure criterion and failure of the intact rock mass, which shows elastic behaviour cannot be detected.

Comparative simulations with the user-defined iso-JRMC model show that for problems like the cut slope it might make a big difference whether the intact rock is defined to be elastic (JR model) or if it underlies the MC failure criterion (iso-JRMC model). In contrast, the material of the intact rock does not have a significant influence if the failure is governed by the jointing itself, as is the case in the tunnel excavation problem.

The comparison of calculation results of simulations with and without the use of the *arc length control* indicates that when working with the JR material model, it is recommended to deactivate the *arc length control* to eliminate the possibility of a premature failure.

The presented thesis discussed material sets with a single joint family only, and a water level was not considered. The outcome of this work can serve as a basis for further studies that include investigations of multiple joint sets and the behaviour of in presence of water flowing in joints.

7 Literature

Bonnier, P; Brinkgreve, R (2013)
Jointed Rock model with overall Mohr-Coulomb failure criterion

Brinkgreve, R.B.J; Enging, E; Swolfs, W.M (2014) a
PLAXIS 2D Material Models Manual (Anniversary Edition). PLAXIS bv, Delft, The Netherlands.

Brinkgreve, R.B.J; Enging, E; Swolfs, W.M (2014) b
PLAXIS 2D Reference Manual (Anniversary Edition). PLAXIS bv, Delft, The Netherlands.

Goodman, R.E; Bray, J.W. (1976)
Toppling of rock slopes. Proc. Speciality Conference on Rock Engineering for Foundations and Slopes, Boulder, Colorado, ASCE Vol.2.

Goodman, R.E (1989)
Introduction to Rock Mechanics. University of California at Berkley. John Wiley & Sons.

Goricki, A. (1999)
Base Friction Versuche für felsmechanische Kluftkörpermodelle. Diploma thesis, Graz University of Technology.

Graz University of Technology (2007)
Felsmechanik und Tunnelbau. Script, Institute for Rock Mechanics and Tunneling Graz University of Technology.

Hoek, E; Bray, J. W. (1981)
Rock Slope Engineering. The Institution of Mining and Metallurgy, London.

8 APPENDIX

Plastic points in a cantilever after failure due to an applied load (qualitatively)

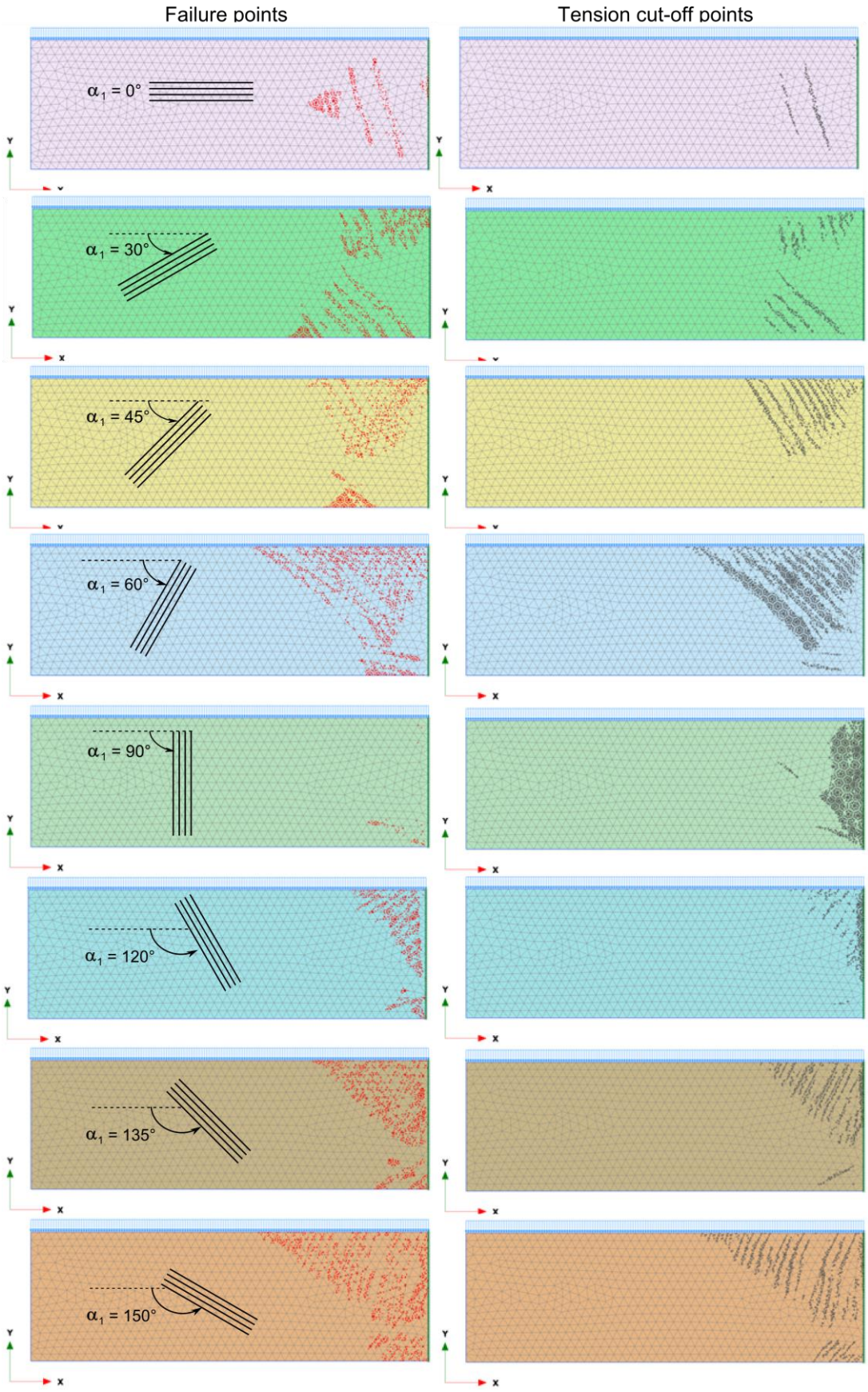

Deformations and plastic points in a cut slope due to a φ/c-reduction (qualitatively)

Material parameters according to section 4.2

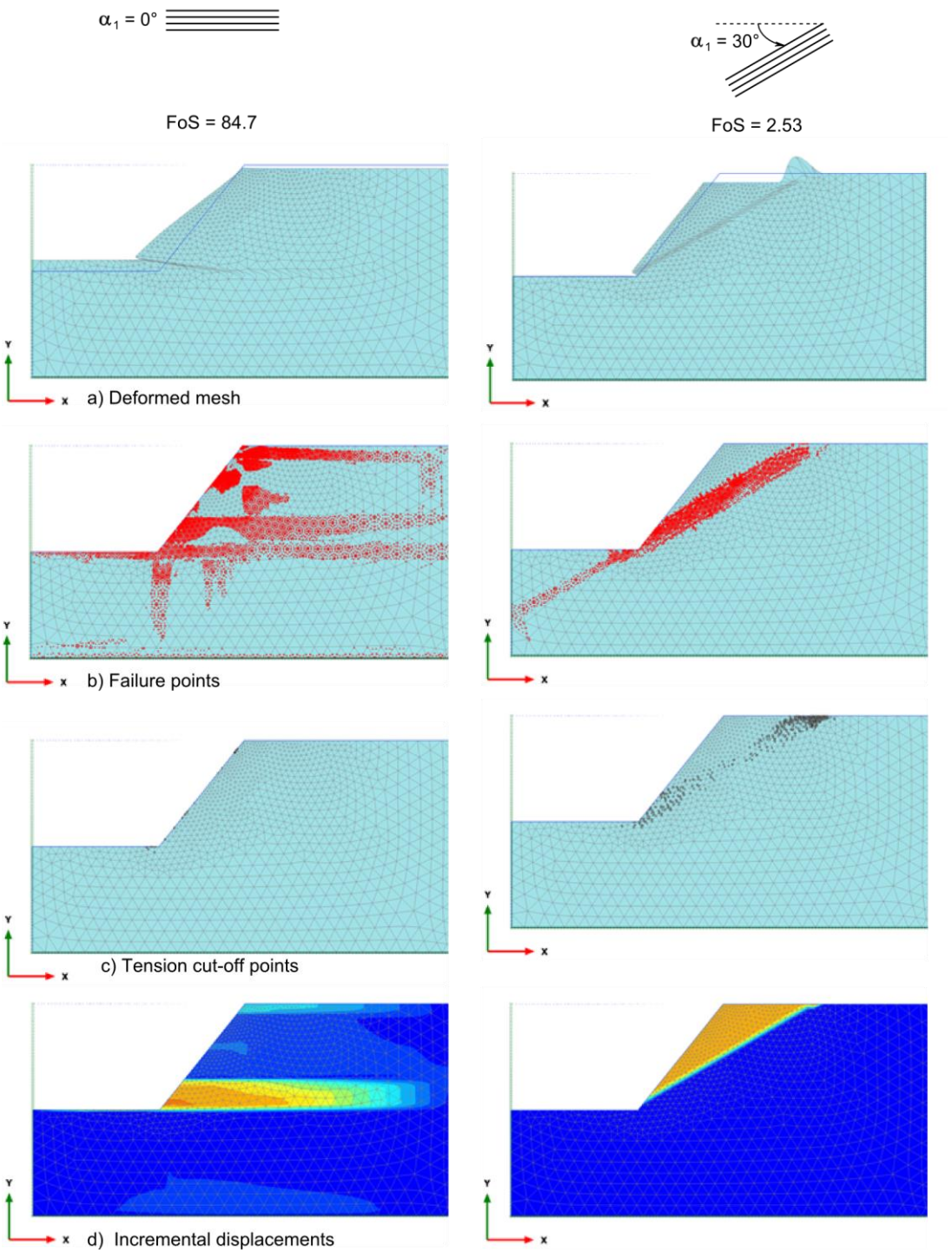

Deformations and plastic points in a cut slope due to a φ/c-reduction (qualitatively)

Material parameters according to section 4.2

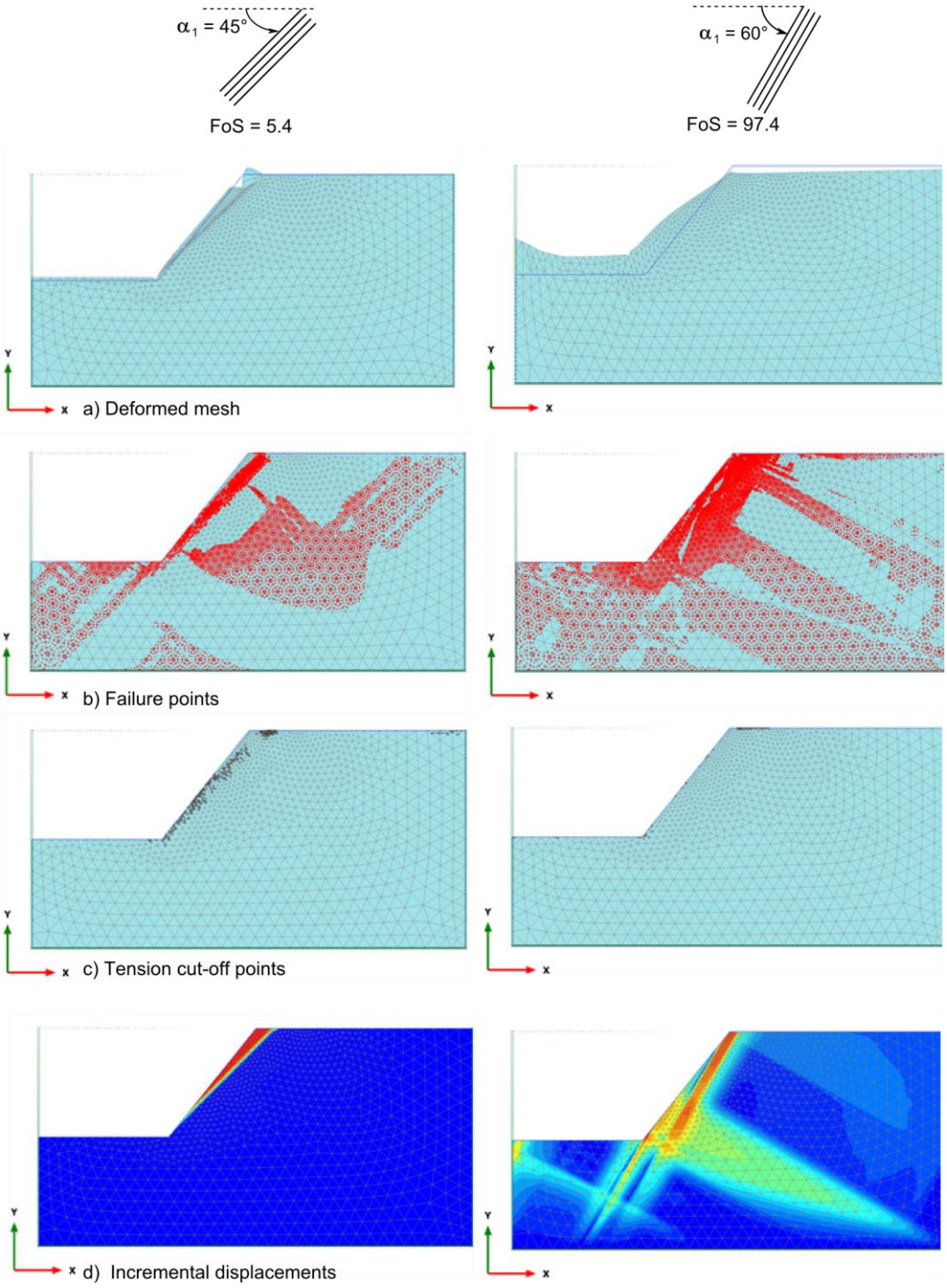

Deformations and plastic points in a cut slope due to a φ/c-reduction (qualitatively)

Material parameters according to section 4.2

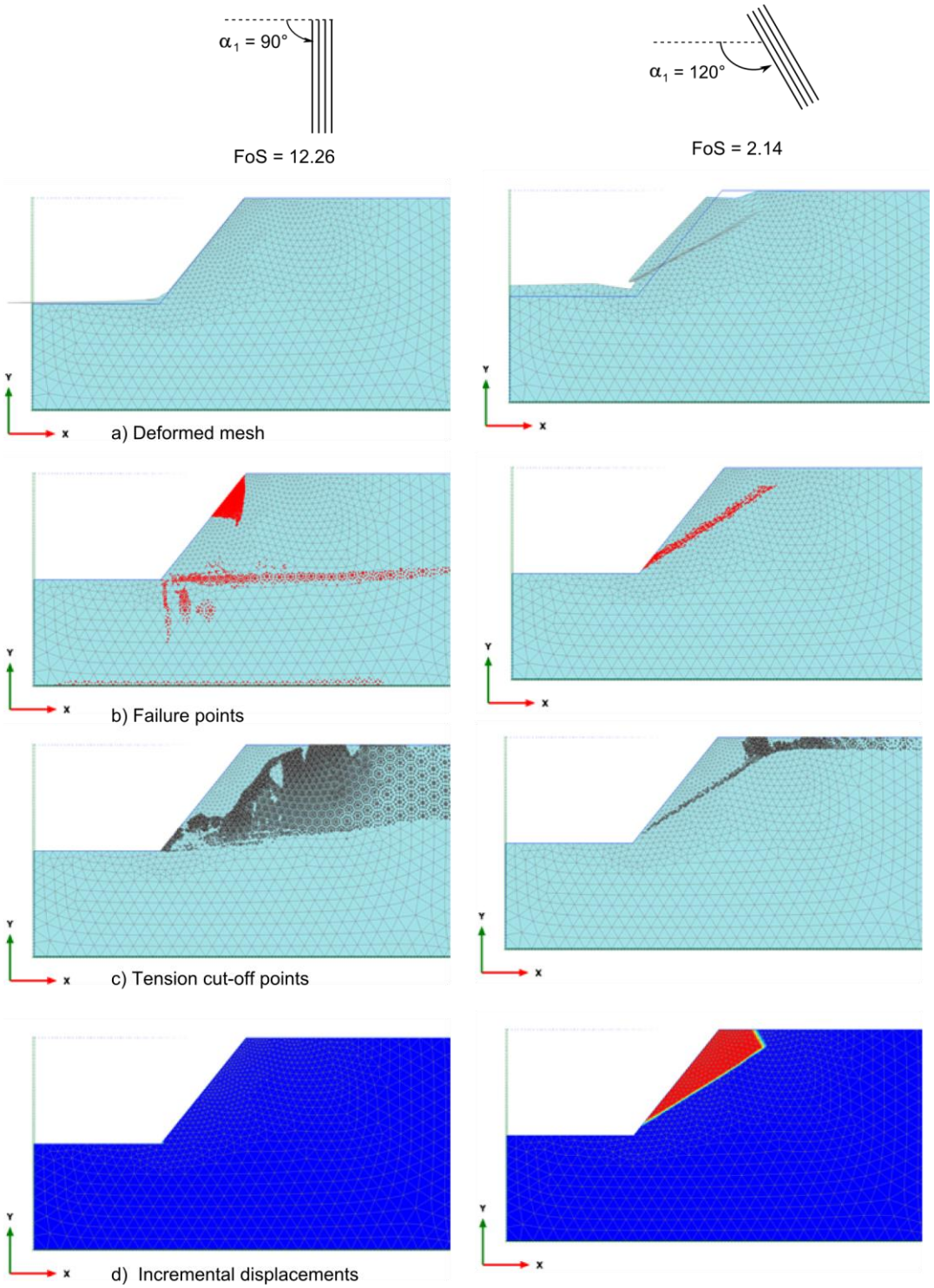

Deformations and plastic points in a cut slope due to a φ/c-reduction (qualitatively)

Material parameters according to section 4.2

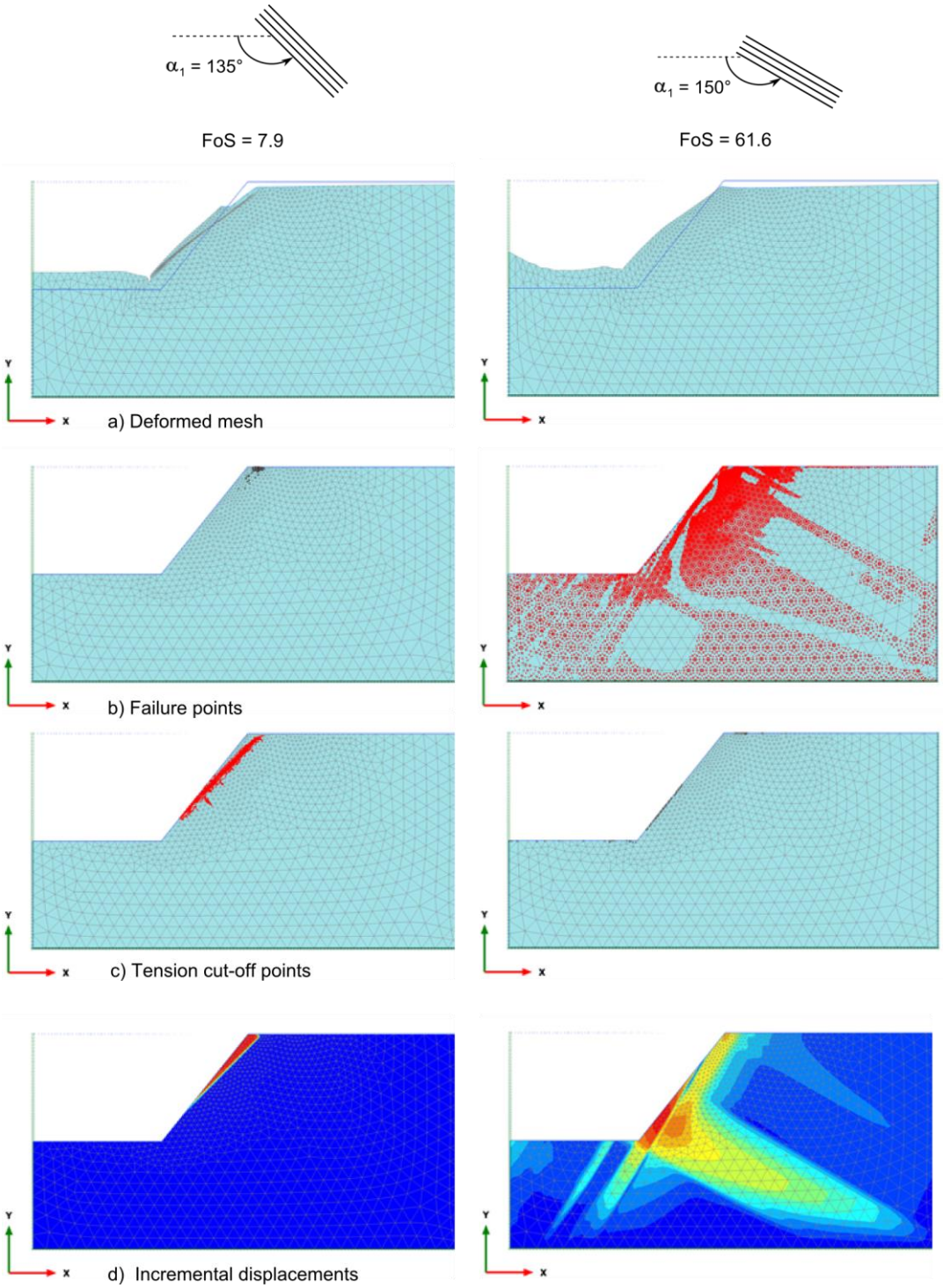

Deformations and plastic points in a cut slope due to an applied load (qualitatively)

Material parameters according to section 4.2

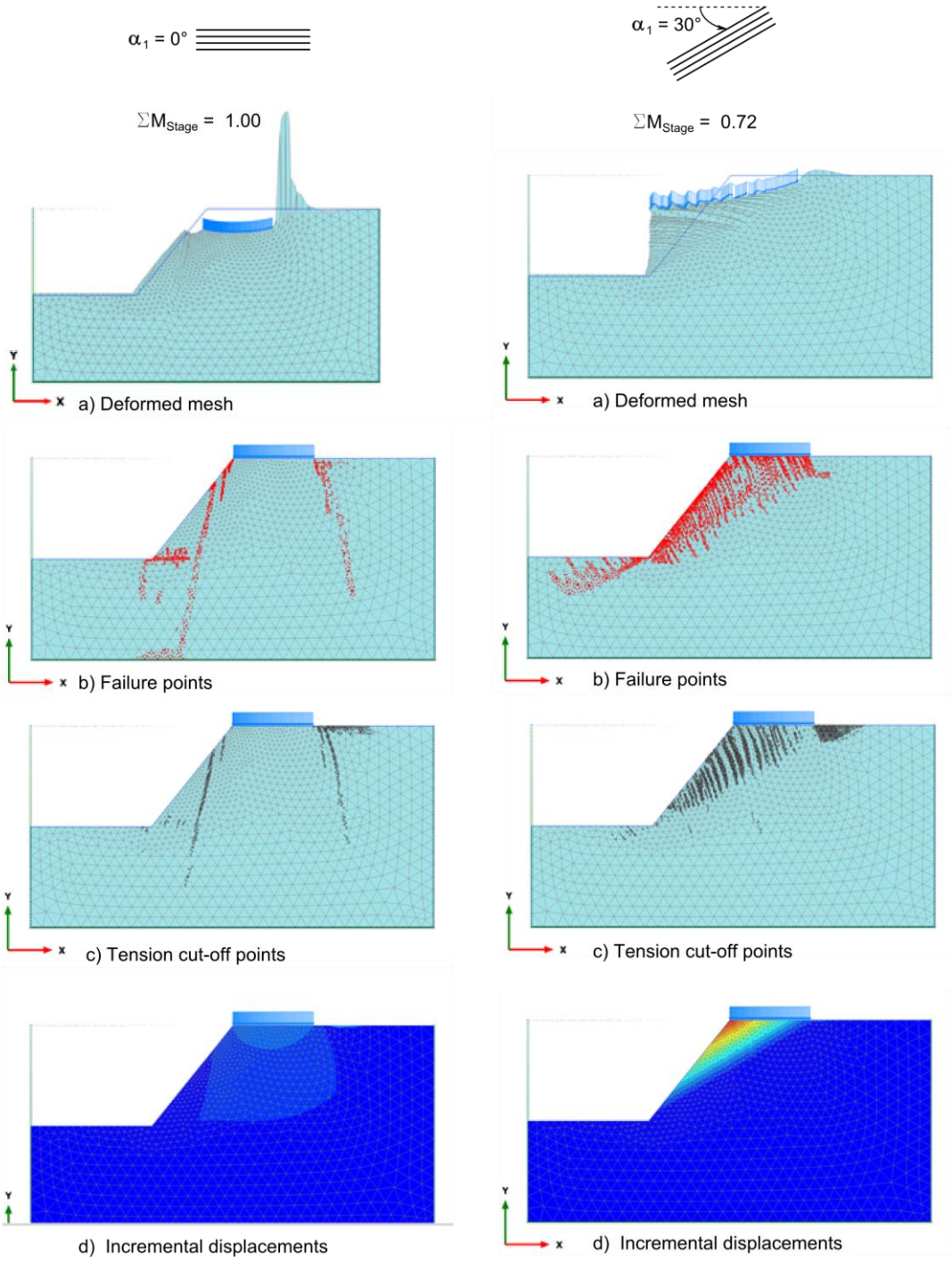

Deformations and plastic points in a cut slope due to an applied load (qualitatively)

Material parameters according to section 4.2

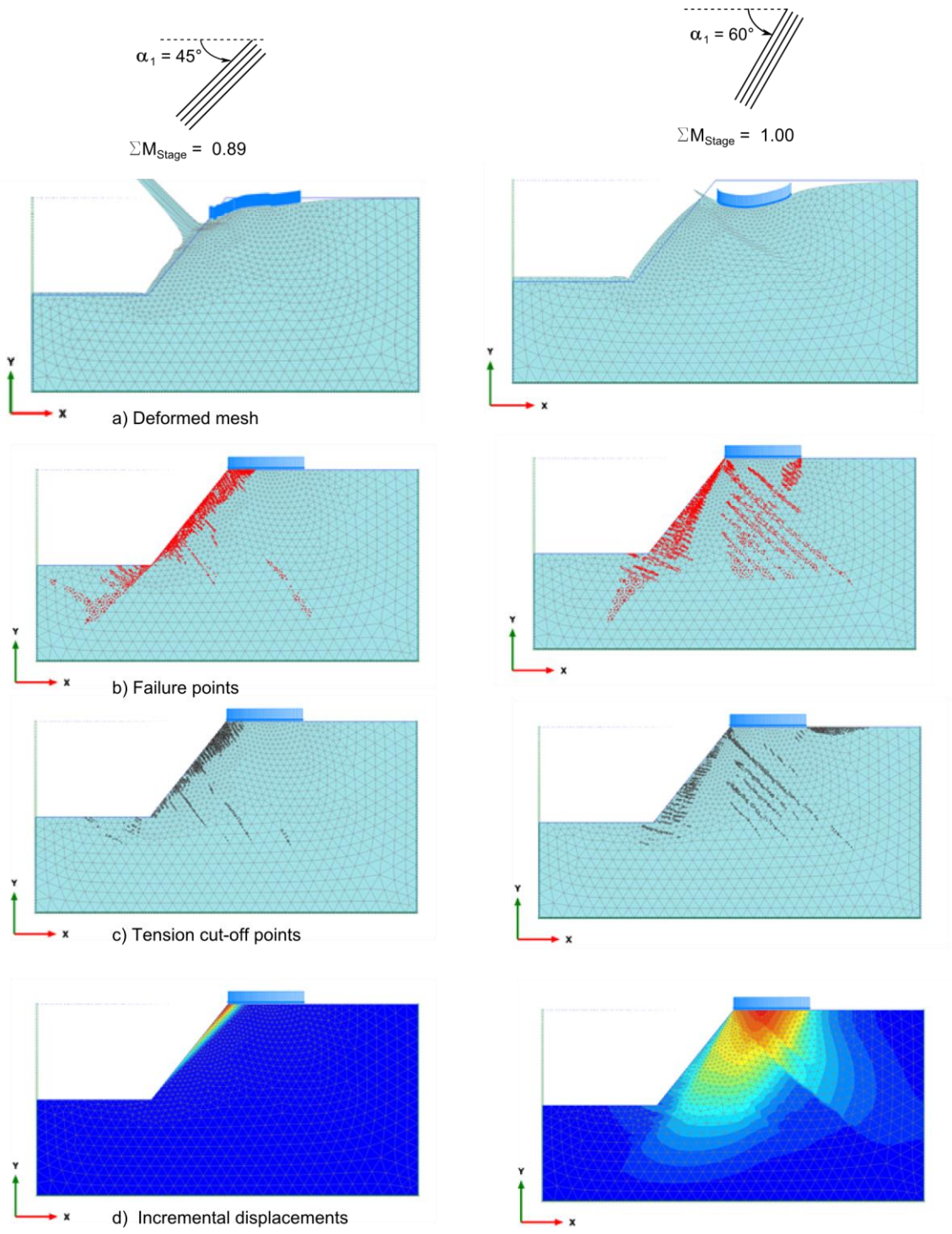

Deformations and plastic points in a cut slope due to an applied load (qualitatively)

Material parameters according to section 4.2

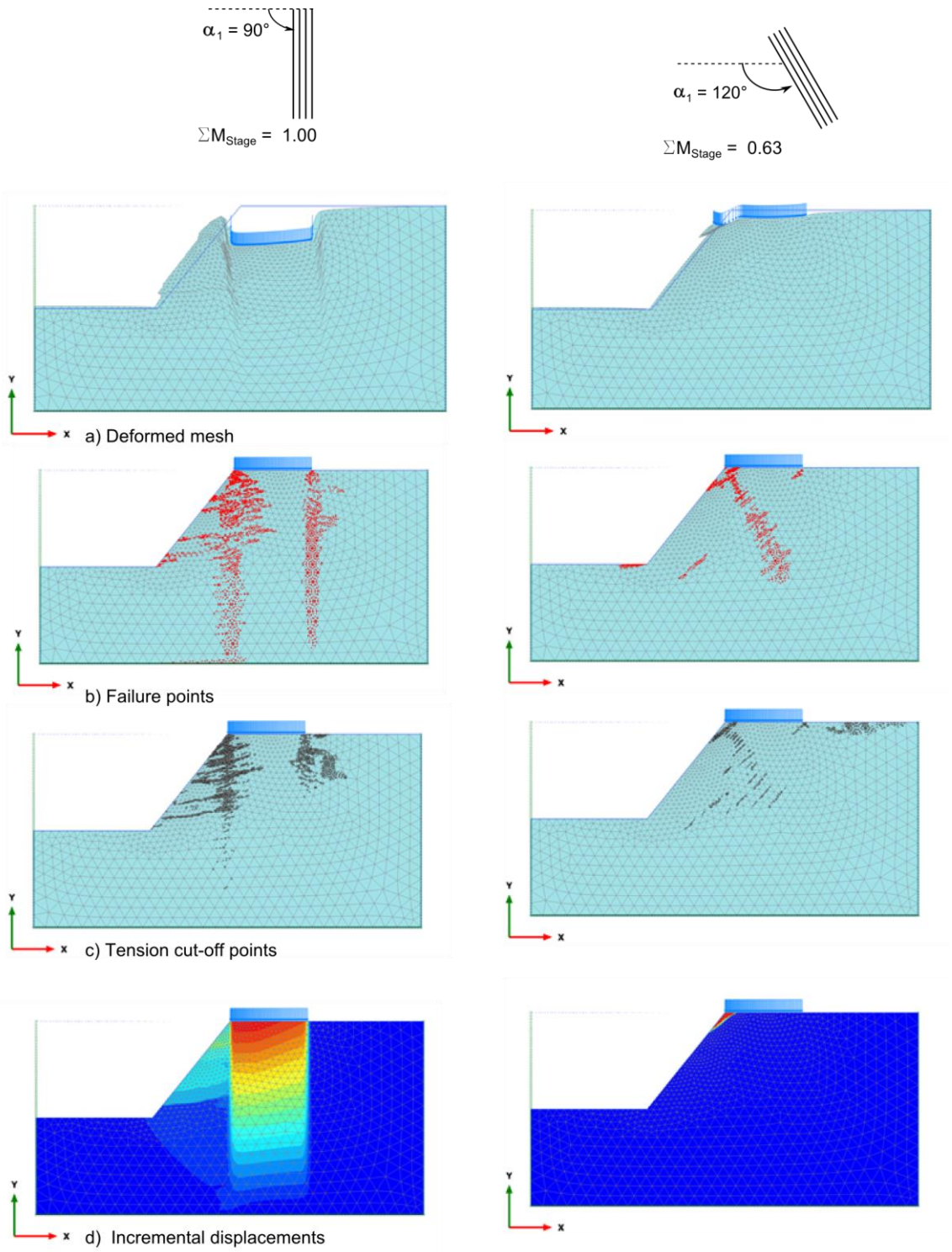

Deformations and plastic points in a cut slope due to an applied load (qualitatively)

Material parameters according to section 4.2